APTD-0960

PB 210 672

DESIGN CONSTRUCTION AND EVALUATION OF A MOBILE LIDAR SYSTEM FOR THE REMOTE MEASUREMENT OF SMOKE PLUME OPACITY

FINAL REPORT

EEI RESEARCH PROJECT RP39 AND
EPA CONTRACT NO. 68-02-0093

C.S. COOK
G.W. BETHKE

SPACE SCIENCES LABORATORY

Reproduced by
NATIONAL TECHNICAL INFORMATION SERVICE
U.S. Department of Commerce
Springfield VA 22151

SPACE DIVISION
GENERAL ELECTRIC

95.

4 - 2178

BIBLIOGRAPHIC DATA SHEET	1. Report No. APTD-0968	2	3. Recipient's Accession No.

4. Title and Subtitle
Design Construction and Evaluation of a Mobile Lidar System for the Remote Measurement of Smoke Plume Opacity

5. Report Date
December 1971

6.

7. Author(s)
G. S. Cook, G. W. Bethke

8. Performing Organization Rept. No. GE-SD No. 214-A77

9. Performing Organization Name and Address
General Electric Company
Space Division, Space Sciences Laboratory
P. O. Box 8555
Philadelphia, Pennsylvania 19101

10. Project/Task/Work Unit No.

11. Contract/Grant No.
68-02-0092

12. Sponsoring Organization Name and Address
Environmental Protection Agency, Durham, N. C. 27701
and Edison Electric Institute
90 Park Avenue, New York, New York 10016

13. Type of Report & Period Covered
Final

14.

15. Supplementary Notes

16. Abstracts A mobile (truck mounted) ruby laser lidar system has been designed, constructed and evaluated for the remote measurement of smoke plume opacity (or transmittance). The system has been tested at ranges of 211 and 319 meters using synthetic targets of known laboratory measured transmittance. The targets used were made of bright and black anodized aluminum screen, glass, plexiglass, white painted plywood and black felt. These tests indicated an error which increased as target reflectance increased, the reflectance increase being due either to a decrease in transmittance or to an increase in reflectance at a given transmittance. This error was found to be less than + 2.5 percent for target transmittances greater than 0.80 and was less than + 12 percent for target transmittances greater than 0.50. The error was always positive making the lidar measurements always an upper bound measure of transmittance. The transmittance measurement error was found to be largely due to photo-multiplier tube afterpulsing, which, after extensive photomultiplier tube gating investigations, could not be avoided with the then available photomultiplier tubes and lack of detailed understanding of the afterpulsing mechanism. However, two new techniques, one recently available, seem likely to eliminate the afterpulsing problem particularly since the mechanism is now more evident as a result of these investigations, the lidar system was evaluated at two local and three non-local field test sites. Both oil fired and coal fired plumes were observed. In addition to the lidar measurements, at some sites telephotometer measurements of plume transmittance and plume-to-sky contrast were made for comparison purposes. In general, the lidar and telephotometer determined transmittance values agreed within the accuracy expected for a given plume transmittance as indicated by the synthetic target test results. Plume-to-sky contrast (plume visibility) was found to have no correlation with plume transmittance because of the variability of ambient illumination of the plume

17. Key Words and Document Analysis. 17a. Descriptors
Air pollution
Lasers
Smoke
Design criteria
Mobile equipment
Transmissometers
Simulation
Field tests
Steam electric power generation
Fuel oil
Coal
Visibility

17b. Identifiers/Open-Ended Terms

17c. COSATI Field/Group 13B

18. Availability Statement
Unlimited

19. Security Class (This Report) UNCLASSIFIED

20. Security Class (This Page UNCLASSIFIED

21. No. of Pages 100

22. Price $4.95

DESIGN, CONSTRUCTION AND EVALUATION OF A MOBILE LIDAR SYSTEM FOR THE REMOTE MEASUREMENT OF SMOKE PLUME OPACITY

Final Report

Period Covered: December 24, 1969 to December 21, 1971

EEI Research Proj. RP39 - GE-SD Requisition No. 214-A77

EPA Contract No. 68-02-0093 - GE-SD Req. No. 028-N52

Prepared by: C. S. Cook and G. W. Bethke
General Electric Company
Space Division
Space Sciences Laboratory
P. O. Box 8555
Philadelphia, Pa. 19101

Details of illustrations in this document may be better studied on microfiche

Prepared for: Environmental Protection Agency
Durham, North Carolina 27701

and

Edison Electric Institute
90 Park Avenue
New York, New York 10016

ABSTRACT

A mobile (truck mounted) ruby laser lidar system has been designed, constructed and evaluated for the remote measurement of smoke plume opacity (or transmittance).

The system has been tested at ranges of 211 and 319 meters using synthetic targets of known laboratory measured transmittance. The targets used were made of bright and black anodized aluminum screen,glass, plexiglass, white painted plywood and black felt. These tests indicated an error which increased as target reflectance increased,the reflectance increase being due either to a decrease in transmittance or to an increase in reflectance at a given transmittance This error was found to be less than + 2.5 percent for target transmittances greater than 0.80 and was less than + 12 percent for target transmittances greater than 0.50. The error was always positive making the lidar measurements always an upper bound measure of transmittance.

The transmittance measurement error was found to be largely due to photomultiplier tube afterpulsing, which, after extensive photomultiplier tube gating investigations, could not be avoided with the then available photomultiplier tubes and lack of detailed understanding of the afterpulsing mechanism. However, two new techniques, one recently available, seem likely to eliminate the afterpulsing problem particularly since the mechanism is now more evident as a result of the investigations during this program.

The lidar system was evaluated at two local and three non-local field test sites consisting of Philadelphia Electric Company and Allegheny Power and Light

Company power stations. Both oil fired and coal fired plumes were observed. In addition to the lidar measurements, at some sites telephotometer measurements of plume transmittance and plume-to-sky contrast were made by EPA personnel for comparison purposes. In general, the lidar and telephotometer determined transmittance values agreed within the accuracy expected for a given plume transmittance as indicated by the synthetic target test results. Plume-to-sky contrast (plume visibility) was found to have no correlation with plume transmittance because of the variability of ambient illumination of the plume.

TABLE OF CONTENTS

Page

ABSTRACT

1. INTRODUCTION 1

1.1 The Lidar Concept 1

1.2 Measurement of Plume Transmittance by Lidar 2

1.2.1 Historical Development of the Technique 2

1.2.2 The Single Beam, Single Shot Technique 3

2. MOBILE LIDAR SYSTEM DESIGN 7

2.1 Vehicle and Mount Design 7

2.2 Lidar Design 9

2.2.1 Lidar Optics 11

2.2.2 Lidar Detector and Data Handling Components 14

3. LIDAR SYSTEM TESTS USING SYNTHETIC TARGETS OF KNOWN TRANSMITTANCE. 22

3.1 The Synthetic Targets and Their Laboratory Determined Transmittance 22

3.2 Lidar Target Tests. 26

3.2.1 The Effect of Afterpulsing. 26

3.2.2 Lidar Transmittance Measurements 28

4. FIELD TESTS ON REAL SMOKE PLUMES 44

4.1 Local Field Tests 44

4.2 Field Tests in Western Pennsylvania and West Virginia . . . 46

4.2.1 Tests at Albright, West Virginia 48

4.2.2 Tests at Point Marion, Pennsylvania 52

4.2.3 Tests at Springdale, Pennsylvania 57

Page

5. CONCLUSIONS 61

6. RECOMMENDATIONS 64

7. ACKNOWLEDGEMENTS 68

8. REFERENCES 69

APPENDIX A: THE LIDAR RANGE EQUATION A-1

APPENDIX B: PHOTOMULTIPLIER TUBE GATING INVESTIGATIONS B-1

EXPERIMENTAL TEST METHODS B-3

OFF-GATING METHODS AND RESULTS B-4

Afterpulsing and Focus Electrode Gating of the Amperex 56 TVP B-6

Afterpulsing and Focus Electrode Gating of the RCA 7265 . . . . . B-9

External Grid Gating of the Amperex 56 TVP B-11

External Grid Gating of the RCA 7265 . . . . B-11

Dynode Gating of the Amperex 56 TVP B-13

Dynode Gating of the RCA 7265 . . . . . B-17

DISCUSSION AND CONCLUSIONS. B-17

1. INTRODUCTION

A mobile lidar (light detection and ranging) system has been constructed and evaluated under the joint sponsorship of the Edison Electric Institute (EEI Research Project RP39) and the Environmental Protection Agency (EPA Contract no. 68-02-0093). This system was built for the purpose of remotely monitoring the opacity or transmittance (T) of stationary source smoke plumes. It employs a pulsed ruby laser source and was designed to operate at slant ranges of from 200 to 400 meters. Data has been obtained to a range of 487 meters using a real smoke plume.

1.1 The Lidar Concept

The conventional single ended lidar configuration involves a laser transmitter sending out a short pulse of light ($\sim 10^{-8}$ sec.) from a laser source in conjunction with a receiving system mounted on a parallel or nearly parallel optical axis which collects backscattered light from the outgoing laser pulse as it propagates away from the system. This collected light is focussed on a field-limiting aperture and is then collimated before passing through a narrow band interference filter to a photomultiplier detector. Thus, backscattered light intensity at the receiving aperture is linearly transformed to voltage across the photomultiplier load resistor as a function of time, and thus range.

When the lidar optical path is through the clear atmosphere the backscattered signal at the laser wavelength is made up of two components. These are the component due to molecular (Rayleigh) scattering and that due to aerosol (Mie) scattering. A complete expression for system output voltage as a function of range is shown as equation 15 of appendix A. However, this expression can be simplified

somewhat when considering the relatively short slant ranges at which the plume opacity lidar obtains data. For these ranges attenuation of the beam and atmospheric density changes can be neglected, with the correct expression for system output voltage being

$$V = \frac{c A S E_o E R}{2 r^2} \left[n(r) \cdot \sigma_R (180^o) + m(r) \cdot \sigma_M (180^o) \right] . \qquad (1.1)$$

Here c is the velocity of light, A is the area of the receiving aperture, S is the photomultiplier sensitivity (amps/watt), E_o is the overall system optical efficiency, E is the laser output energy, R is the load resistance, r is the range, $n(r)$ is the number density of molecular scatterers, $\sigma_R (180^o)$ is the Rayleigh backscattering cross section for air, $m(r)$ is the mass concentration of aerosols (μ gm/m^3) and $\sigma_M (180^o)$ is the mass normalized aerosol (Mie) backscattering cross section.

If $n(r)$ and $m(r)$ are constant with range then the bracketed term of equation (1.1) is a constant atmospheric backscattering coefficient, k_s, and equation (1.1) becomes

$$V = \frac{c A S E_o E R}{2 r^2} \cdot k_s , \qquad (1.2)$$

indicating a basic $1/r^2$ dependence of the system signal.

1.2 Measurement of Plume Transmittance by Lidar

1.2.1 Historical Development of the Technique

Prior to the construction and evaluation of the lidar system described in this report consideration had been given to various techniques for

remotely obtaining plume transmittance using both active lidar techniques and passive telephotometer techniques. Basic work by W. D. Conner and J. R. Hodkinson relative to the optical properties of plumes supported jointly by the Public Health Service and the Edison Electric Institute is described in reference 1. They discuss the use of lidar for plume transmittance measurements employing the technique of observing atmospheric backscattering from a range just beyond the plume on consecutive lidar shots; first through the plume and then adjacent to the plume. In addition, early studies of lidar techniques for measuring plume transmittance were conducted at Stanford Research Institute[2] funded by the Edison Electric Institute. These studies involved the use of three basic techniques for determining plume transmittance; consecutive lidar shots through and adjacent to the plume, a dual beam lidar with simultaneous beams through and adjacent to the plume and a single beam, single shot technique involving the observation of light scattering from just in front of and just beyond the plume. This latter technique was examined experimentally using an existing lidar system and synthetic targets of known transmittance. Following this, a contract was awarded to the General Electric Company's Space Sciences Laboratory by the Edison Electric Institute for the development and construction of the present mobile lidar system employing the single beam, single shot technique. Further, following completion of the system the present contract was awarded by the Environmental Protection Agency for an evaluation of the system's performance using synthetic targets of known transmittance as well as real smoke plumes.

1.2.2 The Single Beam, Single Shot Technique

Although the SRI experimental work[2] had pointed out a "receiver

paralysis" problem associated with this technique, it was felt that the system simplifications associated with the technique as well as the possibility of getting around the paralysis problem with receiver gating techniques dictated the single beam, single shot approach. The basic technique for obtaining the lidar determined one-way transmittance T_L is illustrated in Figure 1.1.

Figure 1.1 shows a drawing of a lidar return with photomultiplier tube signal voltage plotted against time and thus range. Although the signal voltage is inherently negative it is shown inverted for clarity in this drawing. The laser pulse is initiated in the transmitter and defines t = o for the system. The initiation of this pulse is monitored by a photodiode looking at the laser cavity providing a triggering signal for the system electronics. Since the transmitting and receiving system axes are parallel but not coincident and since the receiving system has a narrow field of view, the backscattered light from the outgoing laser pulse cannot be seen by the receiving system for the first 50 meters or so of range. Following this, the angular field of view of the receiving system combined with the collimated divergence of the laser pulse allows gradual overlap of the two beams with full overlap occurring at a range of approximately 130 meters (0.8 μ sec.). From this point onward the signal return shows a general $1/r^2$ dependence as shown by equation (1.2) as long as the atmospheric scattering coefficient, k_s, is a constant.

Of course a smoke plume means a discontinuous change in k_s which shows up as a sharp signal spike at the range of the plume as indicated in Figure 1.1. The amplitude of this spike can be up to 40 db above the ambient light scatter-

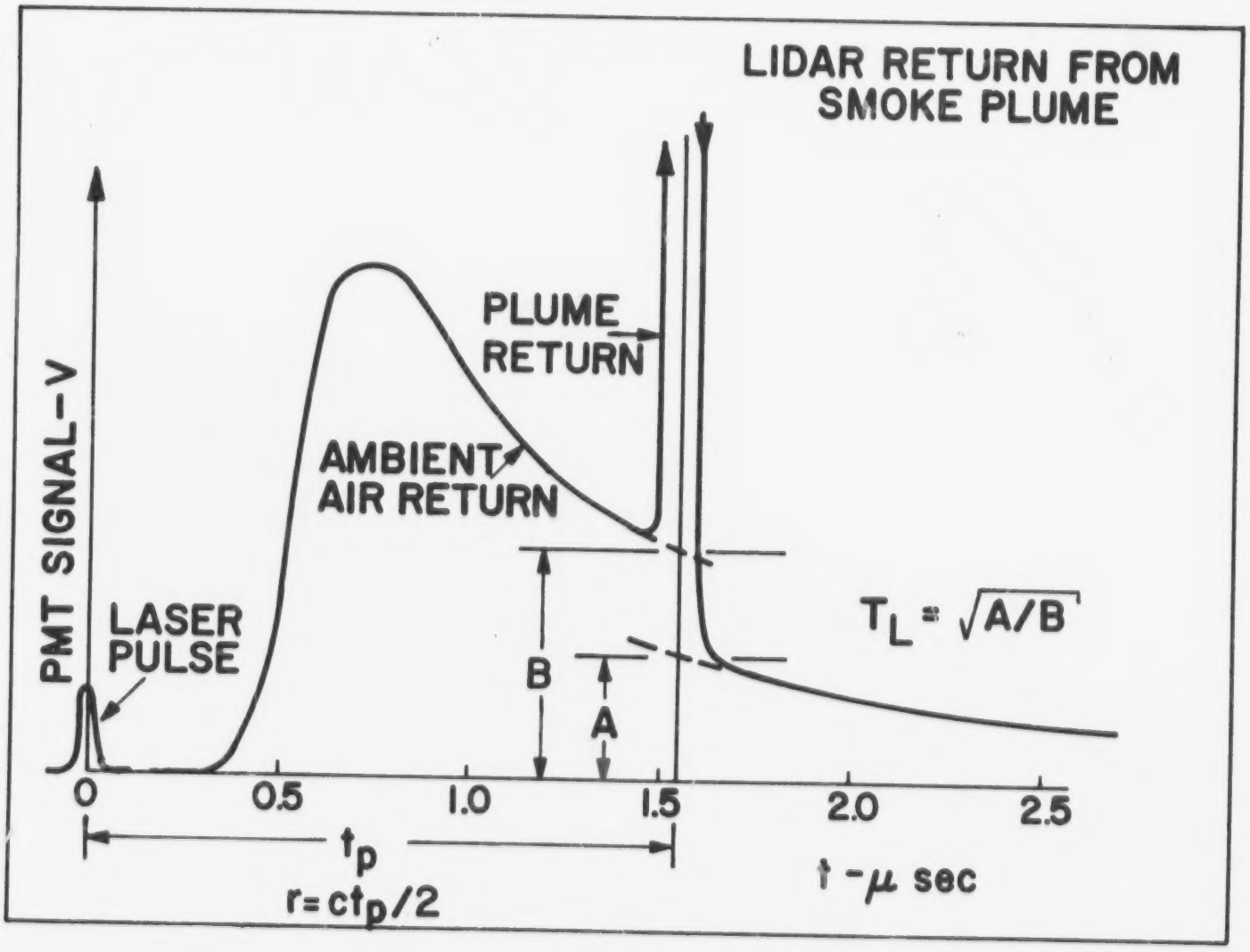

Figure 1.1 A sample lidar return through a smoke plume showing the single beam, single shot technique for obtaining the one way lidar determined transmittance, T_L.

ing for low transmittance highly reflecting plumes. Light scattered to the receiver from ranges greater than the plume will have been attentuated by the plume twice, once going out and once coming back. Therefore the received signal shows a discontinuity at the range of the plume. If the ambient air scattering signal from each side of the plume is extrapolated to a common point in a $1/r^2$ fashion, as shown by the dotted lines in Figure 1.1, the ratio of the two signal levels can be computed as A/B as shown. The one way lidar determined plume transmittance is then given by

$$T_L = (A/B)^{1/2} \tag{1.3}$$

All of this yields an absolute measurement of plume transmittance independent of laser pulse energy provided that k_s is homogeneous in front of and beyond the plume. The measurement is easy in principle but in practice a phenomenon called photomultiplier tube afterpulsing limits the accuracy with which the signal on the far side of the plume can be read. This will be dealt with in detail in Section 3 when test results are discussed.

2. MOBILE LIDAR SYSTEM DESIGN

2.1 Vehicle and Mount Design

As indicated in the proposal, a Ford E-100 Econoline Super-Van was chosen as the vehicle in which to mount the lidar system. Previous experience with another lidar system indicated that the best way to avoid road shock damage to mounted equipment was to rely on the vehicle's suspension, using the softest springing available for the anticipated load to achieve a passenger-car-like ride. The anticipated equipment weight of approximately 1100 lbs. coincided nicely with the 1025 lb. rated payload of the truck selected and the resulting ride is quite smooth. This allowed all of the system components to be hard mounted to the truck body or floor. In a further effort to produce smooth operation an automatic transmission was specified. Since the truck would always be operated fully loaded an extra capacity radiator was specified and since extended storage periods were anticipated a 70 ampere-hour battery was ordered. The color specified was white both for thermal reasons and because it resulted in a white interior for the truck, improving visibility.

Figure 2.1 shows the truck in an operating configuration at the Barbadoes Island Station of the Philadelphia Electric Company. The lidar transmitter and receiver can be seen protruding through the roof opening. The cables going to the portable motor generators can be seen at the rear of the truck. One operator is at the lidar mount aiming the system using the 4-12 power rifle scope while the other operator is seated in front of the oscilloscope controlling the data collection and laser firing. The two roof doors, shown in their open position, are made of

Figure 2.1 Mobile lidar system shown in operating configuration at the Barbadoes Island Station of the Philadelphia Electric Company.

aluminum and when open expose a 6 1/2 by 4 1/2 foot opening in the roof. This modification was performed by the Allegheny Body Company of Philadelphia, a fabricator of custom truck bodies.

The lidar transmitting and receiving assembly is attached to a Quick Set Corporation Model 6222 Geared Head combined with a Model 6800 Stationary Elevating Pedestal. This mounting configuration is shown in the storage/travel position in Figure 2.2 and in an operating position in Figure 2.3. The mount allows 360° rotation in azimuth with -5° to 42° elevation allowed for most azimuth angles. In going from the storage/travel to the operating position the whole mount is translated vertically between 15 and 20 inches using the stationary elevating pedestal. The stationary pedestal is bolted to a large aluminum plate which in turn is bolted through the ribbed sheet metal truck floor at points near where the floor is spot welded to the frame cross members. This mounting method has proved quite satisfactory during field use since the pointing accuracy, which need not be high for this application, is limited by overall truck motion on its suspension rather than mount to truck motion. The dexion brace shown supporting the lidar in Figure 2.2 is a removable storage/travel brace and stiffens the lidar mount considerably for travel. This has proved successful in combination with the soft vehicle springing, in that the lidar has retained its optical alignment quite well during extensive road trips including rough secondary roads.

2.2 Lidar Design

The lidar design employed is conventional although refracting instead of the reflecting optics employed in a previous system[3] were used for compactness

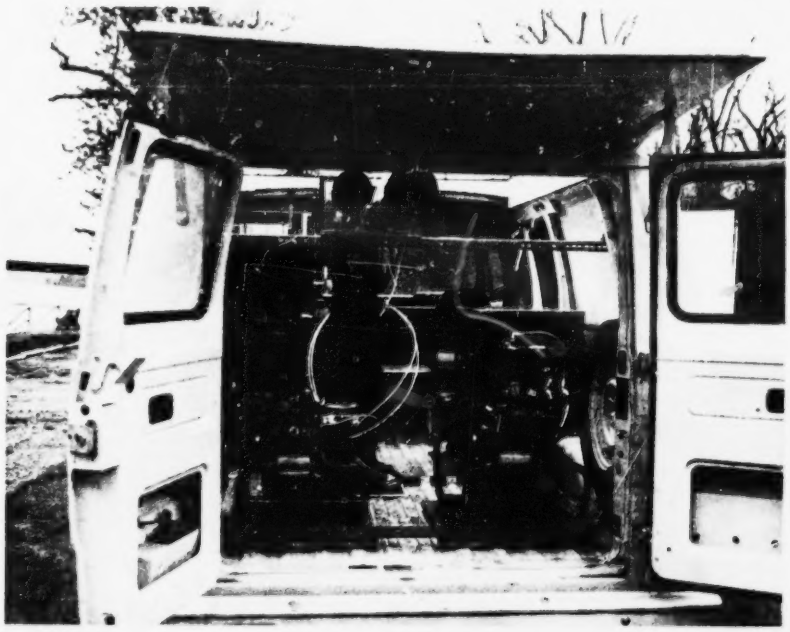

Figure 2.2 Lidar in storage/travel position

Figure 2.3 Lidar in operating position showing lidar mount, laser water cooler and system electronics.

and ease of fabrication. A block diagram of the complete system is shown as Figure 2.4. For purposes of discussion it is convenient to divide the lidar system into its optical and non-optical components.

2.2.1 Lidar Optics

The transmitted laser light pulse originates in a 1.0 cm diameter 7.6 cm long ruby crystal installed in a Hadron/TRG Model 200B laser head. The laser characteristics as well as the remaining system optical characteristics are shown in Table 2.1. The laser is Q-switched by means of a rotating prism rear reflector yielding 30 nanosecond wide pulses (FWHH). The front cavity reflector is a single sapphire resonant reflector (etalon) of about 27% reflectivity, a more durable design than the more common dielectric coated reflectors. Th cavity gain is further increased by aligning the flat ends of the laser rod with the output reflector. Single pulse output of up to 1.0 joules is obtained without the use of a dye cell accessory.

The laser pulse is then collimated using a Galilean telescope reducing its divergence from the 5 milliradians or less characteristic of the laser cavity to approximately 0.5 milliradians full angle at the half power points. The negative lens is plano-concave with the plane side facing the laser so that no focussed laser reflection will cause a thermal distortion of the optical path. The positive lens is a 5 inch air spaced, coated achromat of 25 inch focal length.

The backscattered light is collected by a 6 inch diameter f/5 air spaced, coated achromat and focussed on a field stop with 4 milliradian field of view. Light emerging from this field stop is collimated by a 2.14 inch focal length

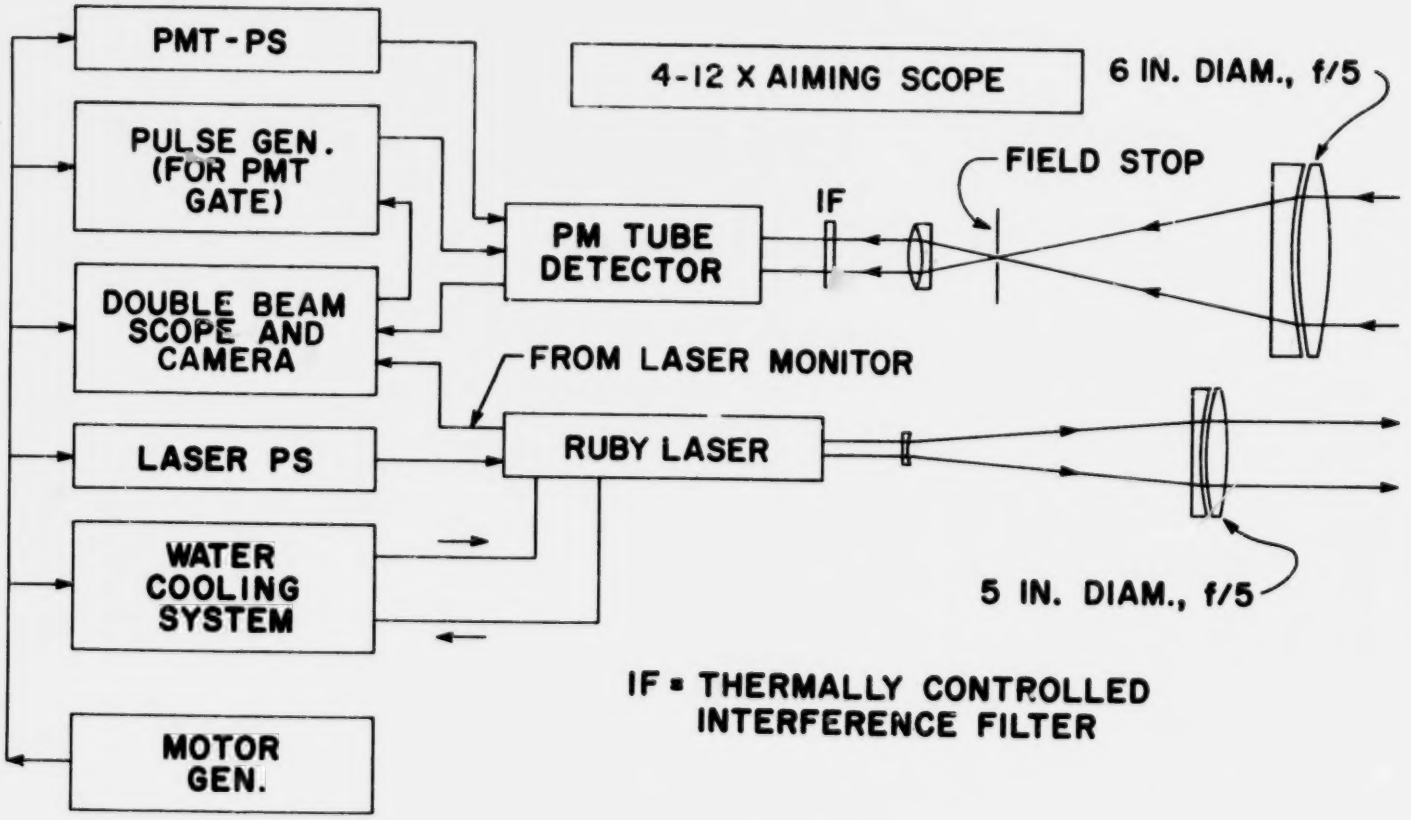

Figure 2.4 Block diagram of mobile lidar system

TABLE 2.1 Lidar Optical Characteristics

Laser	
Manufacturer and Model:	Hadron/TRG Model 200B/104A
Type:	Rotating prism Q-switched ruby
Output Wavelength:	6943A
Maximum Output Energy:	1.0 joule Q-switched
Pulse Width (FWHH):	< 30 nanoseconds
Ruby Rod:	1.0 cm x 7.6 cm
Beam Divergence:	< 5 mrad. (full angle - 1/2 power)
Repetition Rate:	0 - 3 ppm
Cooling:	Deionized water
Laser Collimation	
Collimated Beam Diameter:	10 cm
Collimated Beam Divergence:	~ 0.5 mrad. (full angle - 1/2 power)
Receiving Optics	
Type:	Refracting
Objective Lens:	6 inch diameter, f/5
Collimating (eye) Lens:	2.14 inch focal length
Field of View:	4.0 mrad. full angle
Interference Filter	
Manufacturer:	Infrared Industries
Type:	3 Cavity Interference
Diameter:	2 inches
Transmission Peak Wavelength:	6946.0A (25^{o} C)
Transmission Center Wavelength:	6943.4A (25^{o} C)
Thermal Shift:	+ 0.2 A/^{o} C
Bandwidth (FWHH)	12.0 A
Peak Transmittance:	0.66
Residual Transmittance:	< 0.01%
Filter Rejection:	Far uv to ≥ 1.0 micron
Filter Tilt in Lidar:	0^{o} (perpendicular to radiation)

achromat before it passes to a 3 cavity narrow band pass interference filter placed normal to the optical axis. The filter is temperature controlled by the laser cooling water (in parallel with the laser head) and is generally held at from 20° C to 25° C. The detailed filter characteristics are listed in Table 2.1. Thermal separation of the filter from the laser coolant temperature can be achieved by plugging in a temperature controlled electrical heater tape wrapped around the filter holder. This heater has been preset to control the filter at 30° C. It will do this even with laser coolant flowing at 20° C. After passing through the filter the backscattered light encounters the photocathode of the photomultiplier tube where primary signal detection occurs.

A 4 to 12 power riflescope for aiming the lidar system is attached to the receiving lens tube and completes the lidar optics. This riflescope can be seen in Figure 2.5 showing the complete transmitting and receiving assembly. All of the optical components are mounted on a common 3/4 inch thick aluminum base plate. The receiving system has built-in lockable adjustments for azimuth and elevation angle with respect to the transmitting system. These are used for aligning the two optical axes. Figure 2.6 shows the transmitting side of the system with the laser cavity, the output reflector (etalon) and the negative collimating lens exposed.

2.2.2 Lidar Detector and Data Handling Components

The major effort in designing, constructing and evaluating this lidar system was centered around the photomultiplier tube detector. As has been mentioned in Section 1.2, in order to make the lidar transmittance measurement, it is

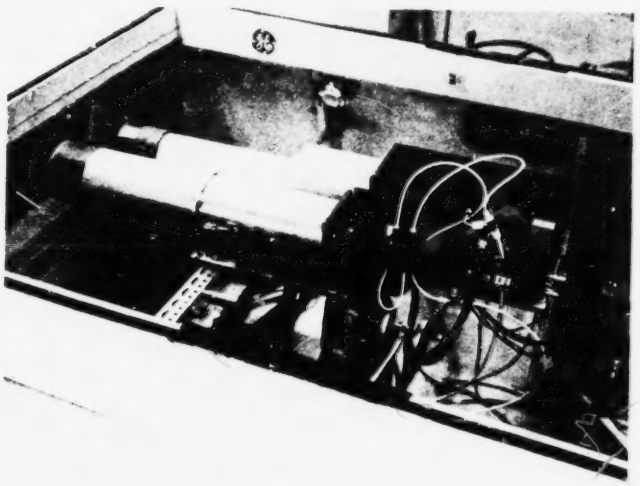

Figure 2.5 Lidar transmitter and receiver in storage/travel position.

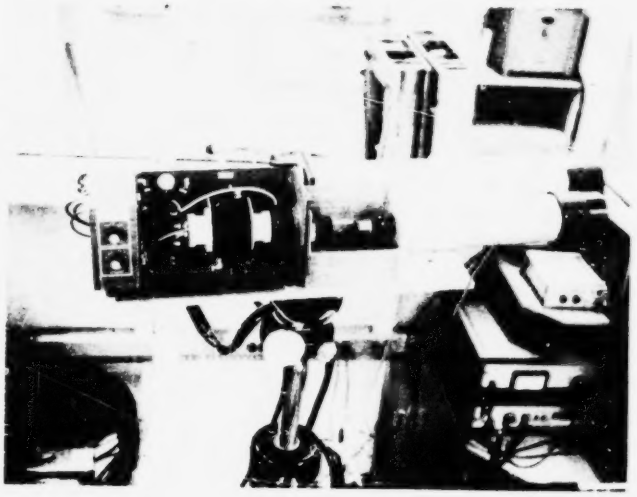

Figure 2.6 Lidar transmitter and receiver in elevated position with laser cavity cover and output window - negative lens cover removed.

necessary to look at a low level signal from the ambient air light scattering on the far side of a plume with good accuracy immediately following the intense return from the plume itself. In order to do this either the detector and the amplifying electronics would have to recover from a signal range of up to 40 db within 100 to 200 nanoseconds or the detector and amplifying electronics would have to be prevented from responding to this intense signal by gating for the duration of the signal. It is difficult to obtain amplifying electronics that will accept such a wide dynamic signal range with the required recovery time even though the stated equipment recovery time per decade when projected over four decades would indicate this. Thus, it was decided that the amplifying electronics should not see the main plume pulse. Further, as has been mentioned, earlier work at Stanford Research Institute[2] had shown the existence of photomultiplier tube afterpulsing related to receiving an intense signal from a plume or an opaque target. They had eliminated these afterpulsing effects by applying a 50 nanosecond wide gating pulse to the focus electrode of their Amperex 56-TVP photomultiplier tube. Accordingly, it seemed best to use this gating technique (for which 30 db plume signal suppression was claimed) since it would get rid of afterpulsing and amplifier saturation effects.

An Amperex 56-TVP tube was purchased and a proper photomultiplier tube tapered voltage divider chain was designed and implemented with consideration given to linear response to hign peak currents (near range scattering), space charge limiting at low voltage per stage, fast response, and coupling a 100 volt gating pulse to the focus electrode. The tube's performance was then evalu-

ated in the laboratory using a pulsed light source in experiments described in Appendix B. Although the ungated tube response to high intensity light pulses was linear to the level expected, the gating response was unacceptable. These results are described in detail in Appendix B but the general results were that 30 db off-gating could not be attained and that increasingly slower tube on-recovery, following removal of the gating pulse, occurred as the off-gating pulse duration was lengthened beyond 100 nanoseconds. It had already been concluded that a minimum practical off-gate width for real plumes, considering plume thickness and laser pulse shape, would be about 200 nanoseconds, so this focus electrode gating technique had to be discarded. An alternative off-gating technique, mentioned by Stanford Research Institute[2], of using a wire mesh grid externally covering the photocathode was also tried in the laboratory even though it was suspected from the focus electrode results that any technique applying strong electric fields near the photocathode would damage the on-response of the tube for realistic off-gating pulse durations. This was confirmed and it suggested that the semi-conductor nature of the photocathode prevented the necessary rapid rate of charge flow required for fast on-response following the integrated result of a charge redistributing electric field.

Since the detailed mechanism of afterpulsing was not understood and since, in any case, it was desirable to prevent the amplifying electronics from receiving the effect of the strong plume pulse it was decided to off-gate the tube by applying the gating pulse to one or more of the early dynodes. The method settled on was to apply a 100 volt pulse to dynodes 2 and 6 which produced off-

gating of greater than 45 db at the projected operating tube voltage of 1500 volts. This then was the configuration first tested on the lidar system and resulted in being the final configuration as well.

It was hoped that this off-gating procedure would eliminate afterpulsing but it did not. Lidar returns from a white building wall used to simulate of plume of zero transmittance and high reflectance showed adequate suppression of the main plume return (shown in detail in Section 3) but also showed a large afterpulsing signal occurring at a time later than the wall signal where the signal return should have been zero. It was then clear that afterpulsing originated somewhere between the photocathode and the beginning of the dynode structure leading to the present supposition that the large number of photoelectrons liberated from the photocathode during the main plume return pulse cause a sufficient amount of ionization of the residual gas or surface ionization in this region to account for the afterpulsing. These ions drift back to the photocathode with a time delay from their formation dictated by their mass and the electric field, and cause secondary electron emission there. The groups of secondary electrons formed then make up the afterpulsing which can probably be prevented only by never allowing the main plume pulse electrons to leave the photocathode. Again, the only methods for doing this available with the Amperex tube had been tried with unacceptable degradation of the on-recovery response of the tube.

It was felt that afterpulsing might depend critically on the detailed design of the photocathode, focus electrode, and first dynode region. Thus, an RCA 7265 photomultiplier tube was substituted and all of the three gating tech-

niques were tried. Although the results (shown in Appendix B) differed in detail from those obtained with the Amperex tube the essential conclusions were the same. Not only was afterpulsing unavoidable but it was more continuous following the main plume pulse allowing no minimal afterpulsing region for measurement as was the case with the Amperex tube. Thus, the RCA tube was removed and the Amperex tube with dynode gating was chosen as the final system configuration.

The remaining detector and system data handling characteristics are shown in Table 2.2. Data recording is done using Polaroid photographs of oscilloscope traces. A double beam oscilloscope is used so that the far side signal from plumes of low transmittance can be displayed at a higher amplification improving reading accuracy. For those cases where single beam presentation is sufficient the remaining beam can be used to display the output of the laser energy monitor if desired. This is handy for keeping track of changes in laser output shot to shot as well as providing the most accurate zero time reference for range measurements. The output energy is monitored by means of a silicon photodiode collimated on the internal volume scattering from the rotating prism and filtered to reject flashlamp light. The photodiode output is available either in integrated form as a calibrated energy monitor or non-integrated as a trigger signal for the system electronics.

When both oscilloscope beams are used for lidar signal presentation the oscilloscope is triggered externally by the non-integrated output of the energy monitor. When the integrated output of the monitor is displayed triggering

TABLE 2.2 Lidar Detector and Data Handling Characteristics

Laser Monitor	
Detector Type:	HP 4220 PIN Silicon Photodiode
Receiving System Detector	
Manufacturer and Type:	Amperex 56 TVP Photomultiplier Tube
Photocathode Type:	S-20
Receiving System Detector Gating	
Gating Method:	+ 100 volt Pulse Applied to Dynodes 2 and 6 of Photomultiplier Tube
Maximum On/Off Ratio:	45.4 db at 1500 volts on PMT
Optical Gating Response:	< 50 nanoseconds
Gating Pulse Generator:	Hewlett-Packard Model 214A
Minimum Pulse Delay:	500 nanoseconds from Laser Trigger
Pulse Width:	Continuously Variable
Data Presentation and Recording	
Oscilloscope:	Tektronix #551 (double beam)
Oscilloscope Preamplifers:	Tektronix Type H (two)
System Risetime:	25 nanoseconds
System Maximum Sensitivity:	0.005 volts/cm

is internal. In either case, the gating pulse generator is then triggered by the gate out of the oscilloscope. This pulse generator is capable of putting out a single 15 nanosecond risetime, $\pm$ 100 volt pulse into a 50 ohm load with continuously variable pulse delay and continuously variable pulse duration. The minimum delay from receipt of trigger is 500 nsec, which, when coupled with an approximately 100 nanosecond oscilloscope delay from receipt of laser monitor trigger signal, yields a minimum range for gating of approximately 90 meters. In practice, the proper gating delay and pulse width is set by first observing the plume return ungated at low sensitivity and then setting the pulse generator for the correct delay.

Finally, the lidar system is powered by two 2.5 kw portable motor generators which are carried in the truck but are removed for operation. The system electronics (oscilloscope, photomultiplier tube power supply and gating pulse generator) are operated on one motor generator while the laser and laser water cooler are operated from the other. This was done to allow the system electronics to operate on surge free power.

3. LIDAR SYSTEM TESTS USING SYNTHETIC TARGETS OF KNOWN TRANSMITTANCE

The mobile lidar system was evaluated using synthetic targets of known transmittance (laboratory measured) to simulate smoke plumes. Although the original intent was to perform these measurements at 200, 300 and 400 meters range, the 400 meter range was not used because of the difficulty of obtaining a suitable 400 meter path length. Instead data was taken at 211 and 319 meters with a greater variety of targets than had been originally planned.

3.1 The Synthetic Targets and Their Laboratory Determined Transmittance

Since it was anticipated that testing would be done at 400 meters range, a target aperture of 42 inches was designed which subtended 2.5 milliradians (full angle) at that range. It was estimated from the laser specification of less than 5 milliradian uncollimated output divergence (full angle, half power) coupled with an experimentally determined divergence curve from an optically similar laser cavity, that the collimated output beam would have greater than 98 per cent of its energy contained within 2.5 milliradians. This would have meant careful aiming at the 400 meter range but allowed a wide variety of target materials because of the common availability of up to 48 inch widths.

Although it was originally planned that targets of 0.50, 0.70 and 0.90 transmittance would be tested, it was easy to expand this to a wider range using aluminum screening, glass and plexiglass in both single and double target configurations. Data was also taken using white and black opaque targets (T = 0), and using the clear target holder aperture (T = 1.00).

The transmittance of the various targets was determined at the laser wave-

length in the laboratory by illuminating the targets from one side with a collimated white light source while viewing the source from the other side of the target with the lidar receiving system. The targets were alternately placed in and out of the beam while the photomultiplier output was read on a Keithly electrometer. This procedure was repeated with the source turned off to see if the front lighting of the targets introduced a significant error in the measurement. It did not, the maximum contribution being less than 1 percent of the reading with the source on. The targets used and their laboratory-measured transmittance values are shown in Table 3.1.

In all cases except the glass, the laboratory measured values agreed well with the expected results. The Plexiglass-G is listed by Rohm and Haas, the manufacturer, to be about 0.92 at this wavelength. The transmittance of the wire screening could be calculated from the wire size and spacing and was in good agreement with the measured values. When questioned, Libby-Owens-Ford stated a value of 0.819 for the transmittance of their Parallel-O-Float glass in 1/4 inch thickness, a value significantly lower than that measured in the laboratory. However, nothing could be found in error in the measurement technique and a repeat measurement confirmed the previous result. In addition, lidar measurements made later on indicated that the laboratory measurement was correct so it was decided to accept the value of 0.861.

Although the lidar measurements could be directly compared with the laboratory transmittance values for the diffusely reflecting screen targets, a subtle difference existed in the case of the specularly reflecting glass and plexiglass

TABLE 3.1 Synthetic Targets Used for Lidar Evaluation

Target Material	Laboratory Transmittance (6943 A)
Plexiglass-G (1/4 inch thick)	0.915
Plexiglass-G (1/4 inch thick)	0.915
L-O-F Parallel-O-Float Glass (1/4 inch thick)	0.861
L-O-F Parallel-O-Float Glass (1/4 inch thick)	0.861
Aluminum Insect Screen	0.640
Aluminum Insect Screen	0.645
50% Open Area Aluminum Screen (Black Anodized)	0.525
50% Open Area Aluminum Screen	0.515
30% Open Area Aluminum Screen	0.288

targets. The specular surface reflections from these materials projected a known fraction of the laser pulse into the reflected direction (deliberately placed off-axis) on the near side of the target. A small fraction of the light scattering return from this reflected path was reflected towards the receiving system and added to that from along the optical axis on the far side of the target, thus influencing the transmittance measurement and giving too high a value. An analysis of this situation was made for the case of a first surface reflectivity, α, and an absorption loss factor per 1/4 inch thickness, β, assuming nearly normal incidence. The result of this analysis is an expression for the backscattered lidar signal ratio, A/B, of the scattered signal from the far side of the target (including near side reflections) to the scattered signal from the near side of the target which is

$$A/B = \alpha^2 + \beta^2 - 4\alpha\beta^2 + 6\alpha^2\beta^2 + 3\alpha^2\beta^4 \qquad (3.1)$$

where higher order terms have been dropped when numerically negligible. Using this relationship and the correct values of α (= 0.0423) and β (= 0.9387) for the glass used, one can compute A/B = 0.7466 with $T = (A/B)^{1/2} = 0.8641$. Here β has been calculated using the laboratory value of T (= 0.861) and the published value of α (= 0.0423). Thus the lidar system should measure a transmittance value 0.36 percent higher than the true one way transmittance of 0.861, a negligibly small difference. An even smaller difference exists for the case of plexiglass where $\alpha \simeq 0.04$ and $\beta \simeq 1.0$. Therefore the lidar determined transmittance values were not corrected for this effect.

3.2 Lidar Target Tests

3.2.1 The Effect of Afterpulsing

A phenomenological description of afterpulsing has been given in Section 2.2.2. Here, the effect of afterpulsing on the lidar signal return is discussed. This is best illustrated by looking at Figure 3.1 which shows a typical lidar return at two amplifications from an opaque, highly reflecting target. The photomultiplier tube signal is inherently negative so the lidar returns are negative going on the oscillogram rather than as drawn in Figure 1.1.

The lower trace, photographed on automatic sweep either before or after the lidar shot, is the differentiated gating pulse, and shows the position and duration of the photomultiplier gating pulse. The uppermost trace shows the lidar signal increasing from zero as beam overlap begins, reaching an off scale maximum and then beginning to fall off in a $1/r^2$ manner until the tube is gated off at which time the signal goes to zero. The white wall "plume" signal then appears even though the response of the tube is down by about 45 db. From this point on the lidar return should be zero, and any further signals must be spurious. Immediately following the removal of the off-gating pulse, early afterpulsing appears and begins falling off to a lower level until the main afterpulsing spike occurs at about 600 nanoseconds. The early afterpulsing and the intermediate minimum can best be seen on the middle trace which has a factor of 10 gain increase over the upper trace. It is clear, that, although the signal shows a 250 to 300 nanosecond period of nearly constant minimum value, that value is not zero as it should be. The form of this afterpulsing is quite repeatable, with the main afterpulse always

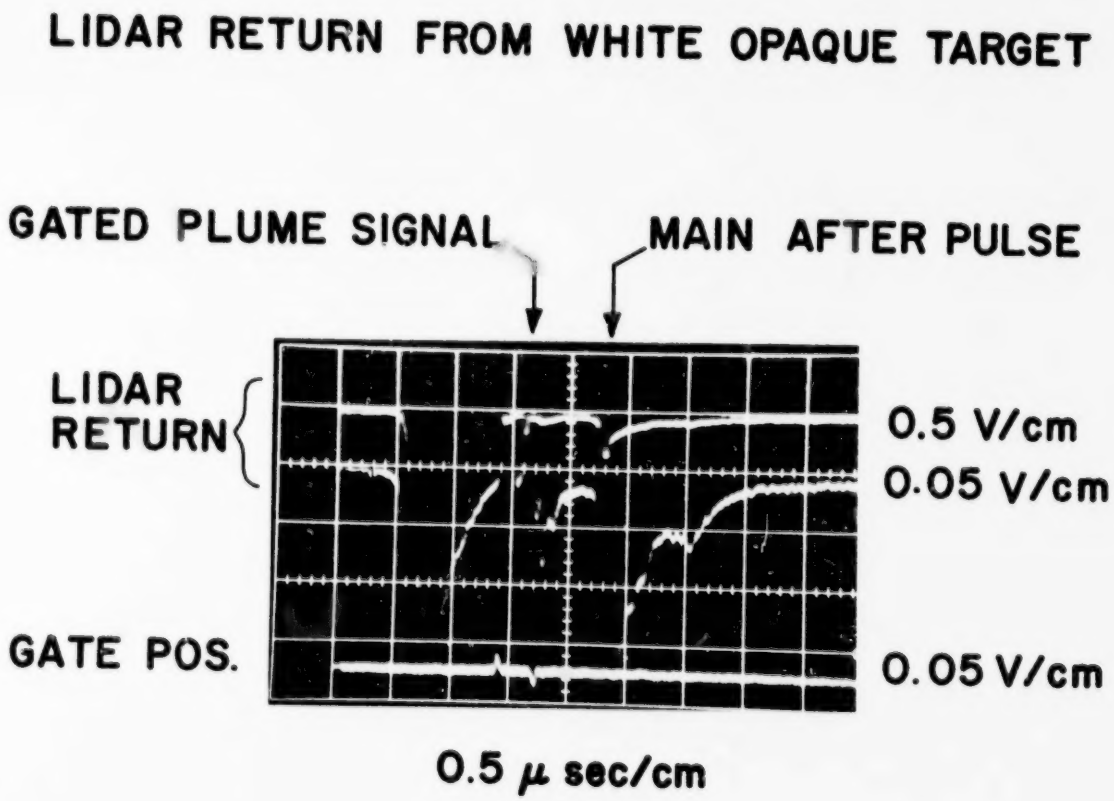

Figure 3.1 A lidar return from a white building wall at a range of about 200 meters. This simulates a plume of zero transmittance and high reflectance.

significantly larger in amplitude than the early afterpulsing. Thus, the transmittance value for targets where afterpulsing is obviously present (as indicated by the main afterpulse) is obtained by using data just preceeding the main afterpulse by 200 to 300 nanoseconds. It will be seen in Section 3.2.2 that as the target reflectance decreases, the afterpulsing-induced transmittance error decreases to the point of becoming negligible at $T \geq 0.80$ or so.

A comparison between lidar returns from white and black opaque targets is shown in Figure 3.2. The plot is double logarithmic so that the basic $1/r^2$ lidar signal return will appear (for a homogeneous scattering atmosphere) as a straight line of slope -2. The sloped lines through the data points are constructed to have a -2 slope and it can be seen that up to the target range the lidar performance is $1/r^2$. The targets used were white painted plywood and a double layer of black felt over plywood. It is obvious that there is a dramatic decrease in afterpulsing going from the white to the black targets, yielding only a factor of 2 reduction in lidar measured transmittance. Closer inspection reveals that while the main afterpulse peak dropped by a factor of about 20, the afterpulsing level near the minimum decreased by only a factor of 4. However, the general shape of the afterpulsing remained the same.

3.2.2 Lidar Transmittance Measurements

Two target holders were constructed with a 42 inch diameter circular aperture and were placed on the roof of a small building at the Valley Forge Space Center and spaced 23 feet apart to simulate plume depth. These are shown on the building roof in Figure 3.3 as used for the 211 meter range data. A corner

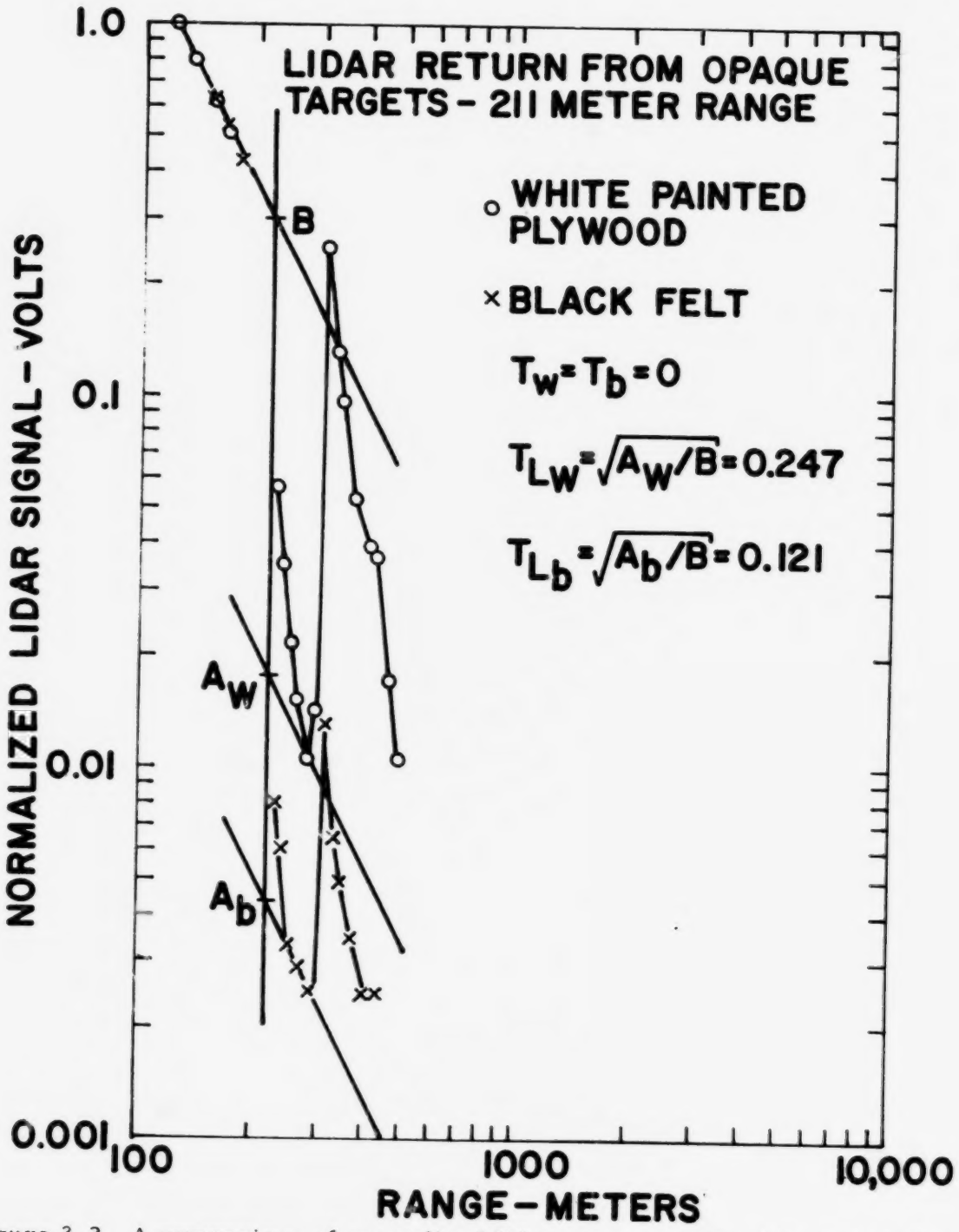

Figure 3.2 A comparison of normalized lidar returns from white and black opaque targets illustrating the relative afterpulsing and resulting values of lidar determined transmittance, T_L.

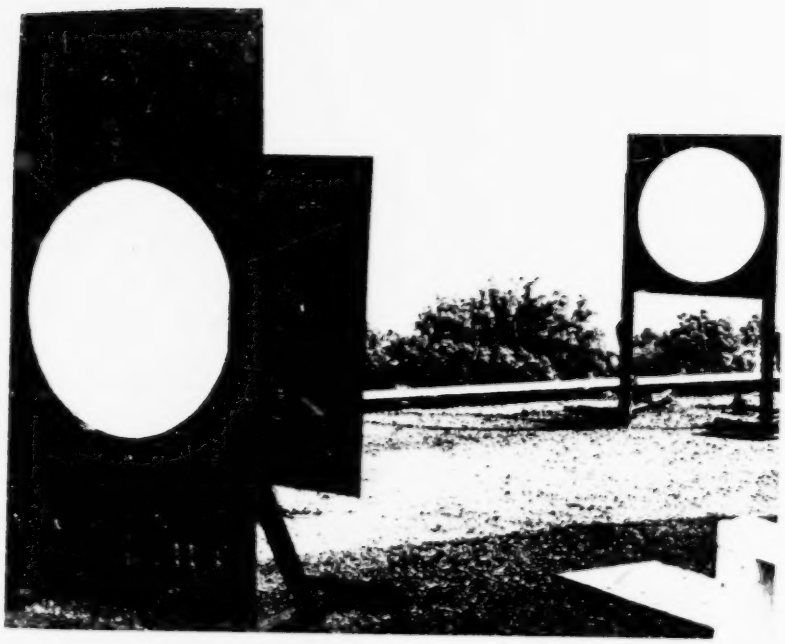

Figure 3.3 Test target holders in position on a building roof at the Valley Forge Space Center. This location was used for the 211 meter range data. The white plywood target is shown in place and was used for alignment purposes.

of the building was used, allowing both targets to be at the roof edge with only the 23 foot path length over the building itself. Although the wisdom of this arrangement was not foreseen, later tests at 319 meters range using a single target located back from the roof edge indicated that atmospheric homogeniety along the optical path was difficult to obtain when a large portion of the path was over and close to building roofs.

For a major portion of the data taking the lidar system was placed 211 meters from the target configuration shown in Figure 3.3. The target holders were arranged so that any specular target reflections were off axis and the targets were not parallel to each other. The lidar system was aligned, using the white gridded target shown, so that the transmitting and receiving axes crossed at 211 meters. This was not necessary in principle, since full overlap of the fields and consequent $1/r^2$ performance begins at about 130 meters range with the axes parallel, but it facilitated aiming the system and was easy to do.

A first check on system performance was made by firing through the clear aperture of both target holders, effectively measuring a target with T = 1.00. The results of this shot are shown in Figure 3.4 with the actual oscillogram shown above the double logarithmic plot of the data. The line through the data points was constructed with a slope of -2 and shows the $1/r^2$ performance on both sides of the target location which is shown by the vertical line. The transmittance measured is unity indicating that the laser pulse was not intercepted by the target holder, the off-gating did not disturb the measurement, and the atmospheric scattering was locally homogeneous on both sides of the target.

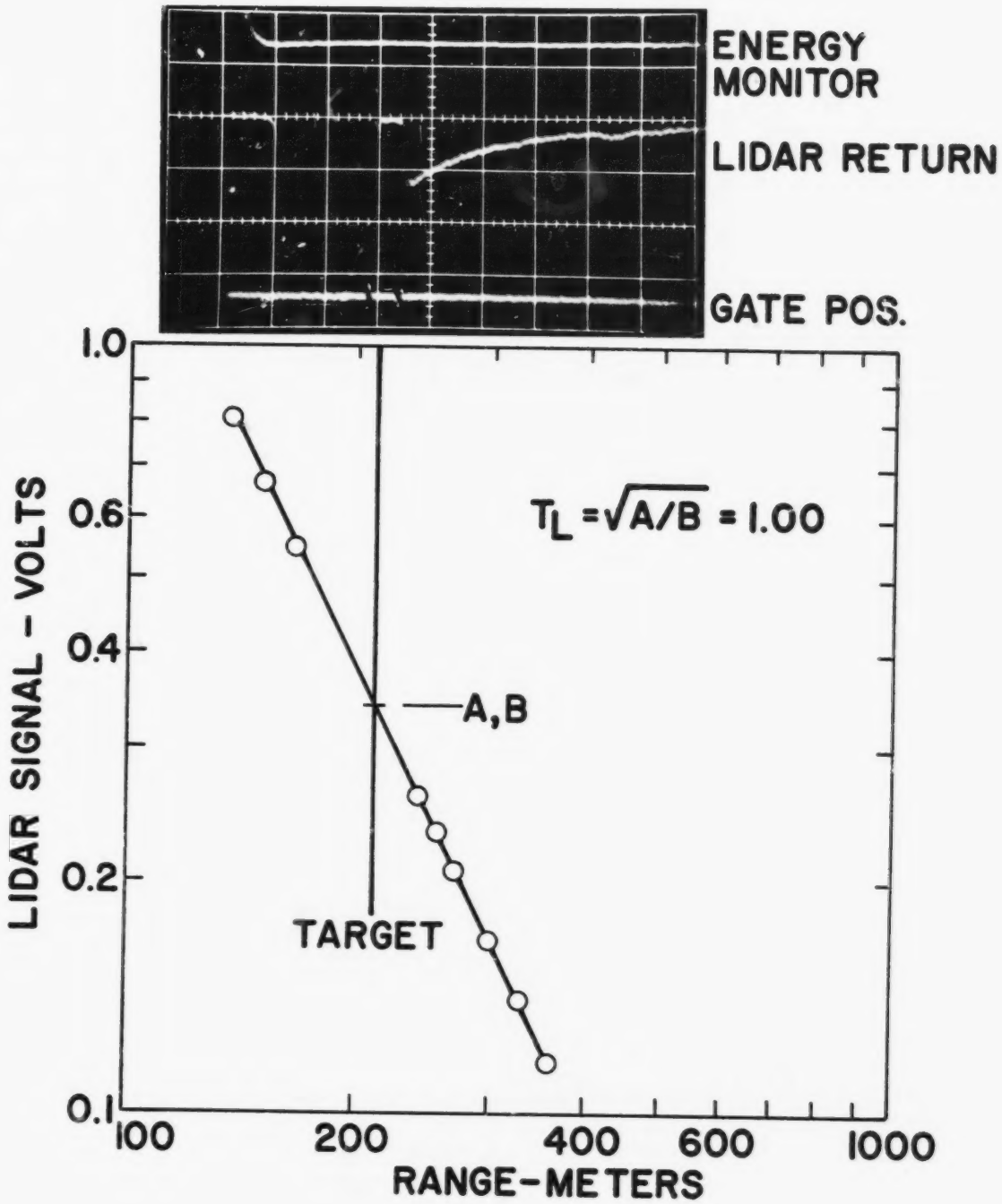

Figure 3.4 Lidar shot through the clear target aperture (T = 1.00) at 211 meters range.

Figure 3.5 shows a typical oscillogram of a lidar shot through two glass targets. Note the absence of any afterpulsing. Again the double log data plot shows good $1/r^2$ performance on both sides of the target and the measured lidar-determined target transmittance (T_L) of 0.757 agrees well with with the laboratory value (T) of 0.741.

A lidar return from a target with high diffuse reflectance is shown in Figure 3.6. The target in this case was two bright aluminum screens with individual transmittances of 0.640 and 0.645 yielding an overall calculated transmittance of 0.412. The reflectance of this target configuration was large enough that the laser pulse could be seen hitting the target with the aid of the sighting riflescope at 10 power even though the target was sunlit. Even though suppressed 45 db by the off-gating of the photomultiplier tube, the main target return pulse can be seen approximately 3.1 oscillogram centimeters from the start of the sweep followed by the start of the main afterpulse at 4.3 oscillogram centimeters from the sweep origin. Far side of the target data was taken in the interval between removal of the off-gating pulse and the start of the main afterpulse and, as can be seen from the plot, it does not exhibit $1/r^2$ behavior. This is due to the presence of the early afterpulsing described in Section 3.2.1. The $1/r^2$ line was drawn through the far side data points in the manner shown in an effort to weight most heavily those points near the target, a policy used throughout the data reduction process even though in this case it gives a worst case answer. It will be seen later on that the problem of thermal lensing with real smoke plumes makes this choice of data weighting advisable. The afterpulsing, then, introduces

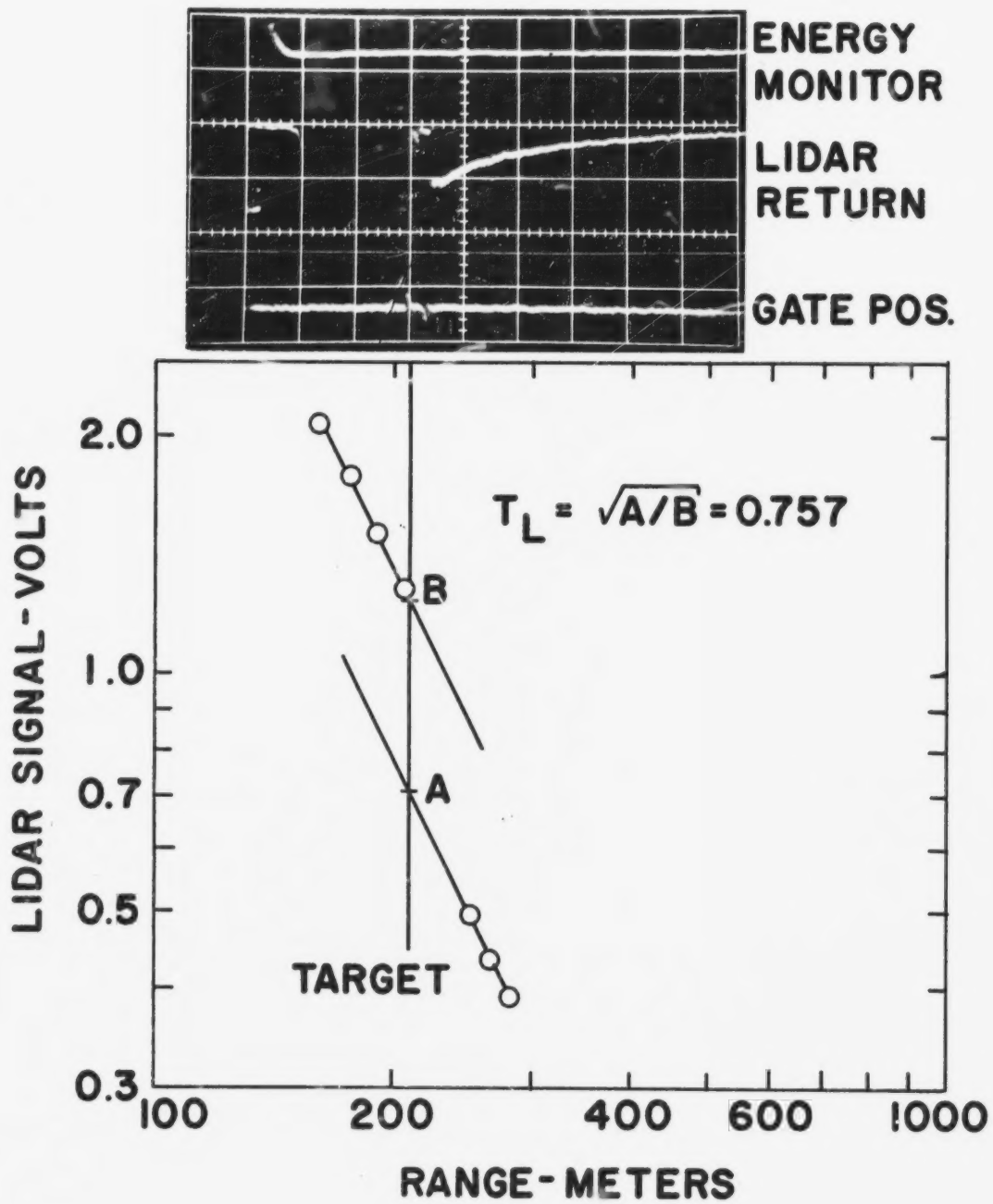

Figure 3.5 Lidar shot through two glass targets (T = 0.741) at 211 meters range.

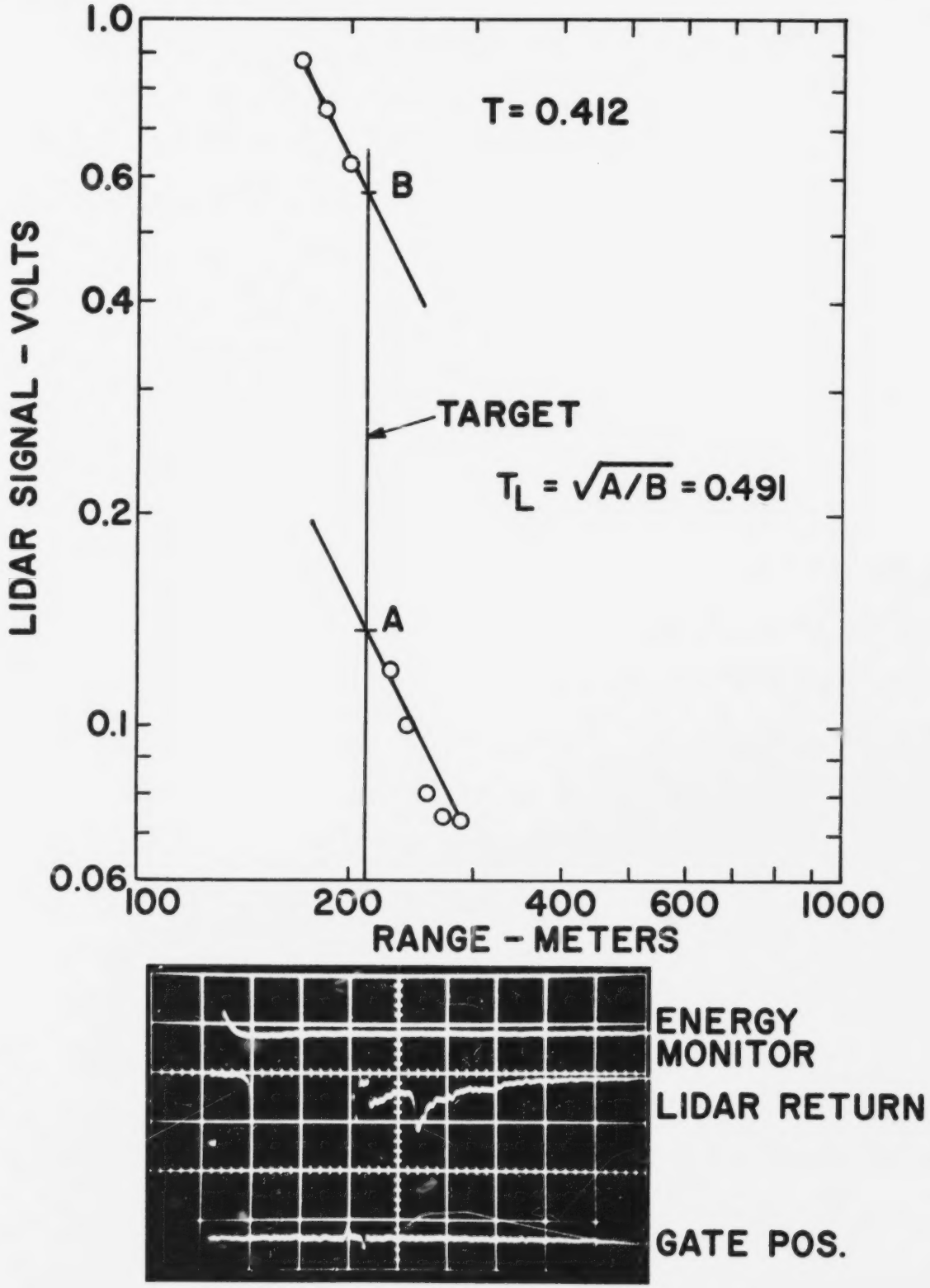

Figure 3.6 Lidar shot through two screen targets (T = 0.412) at 211 meters range.

a substantial error giving a lidar determined transmittance, T_L, of 0.491 as compared with the laboratory measured value of 0.412. If a parallel $1/r^2$ line is constructed through the minimum amplitude data points, a value of $T_L = 0.462$ is obtained, still yielding a substantial error.

A summary of the averaged results for all of the synthetic target testing is shown in Table 3.2. With the exception of the clear aperture and opaque target shots, these data represent the averaging of from two to four lidar shots per data point. As can be seen, results are shown both with and without off-gating.

The results for the 211 meter range are shown in Figure 3.7, the 45 degree line through the origin indicating perfect agreement. The most obvious feature of the results is that off-gating the photomultiplier tube significantly improves the system accuracy even though, as mentioned previously, it does not prevent afterpulsing. This improvement must be due to not overdriving the amplifying electronics when off-gating is used. Although the stated and measured risetime per decade of 25 nanoseconds yields only a 75 nanosecond response time when extrapolated to 3 decades, it is clear that this extrapolation cannot be made over such a wide dynamic range and that the real recovery time over this signal range is longer. The detailed mechanism of this slow recovery was not identified.

Next, it can be seen by considering the open circled points connected by the curve, that as the target transmittance decreased there was a continuous increase in measurement error. This is really due to the attendant increase in target reflectance and thus, afterpulsing. The solid circle points illustrate the reduction in measurement error obtained at a given target transmittance by

TABLE 3.2 Averaged Results of Lidar Measurements of Target Transmittance

Target and Configuration	Target Range	Lab. Transm.	Gated Off ?	Avg. lidar Transm.
Clear aperture	211 m	1.00	Yes	1.00
1 Plexiglass sheet	"	0.915	No	0.956
" " "	"	"	Yes	0.925
1 glass sheet	"	0.861	No	0.891
" " "	"	"	Yes	0.861
1 - insect screen	"	0.640	No	0.758
" " "	"	"	Yes	0.672
1 - 50% black screen	"	0.525	No	0.609
" " " "	"	"	Yes	0.561
1 - 50% screen	"	0.515	No	0.685
" " "	"	"	Yes	0.573
1 - 30% screen	"	0.288	No	0.521
" " "	"	"	Yes	0.409
2 Plexiglass sheets	"	0.837	No	0.914
" " "	"	"	Yes	0.880
2 glass sheets	"	0.741	No	0.762
" " "	"	"	Yes	0.742
2 - insect screens	"	0.412	No	0.659
" " "	"	"	Yes	0.506
White plywood	"	0	Yes	0.247
Black felt	"	"	Yes	0.121
Clear aperture	319 m	1.00	No	0.961
1 Plexiglass sheet	"	0.915	No	0.959
" " "	"	"	Yes	0.908
1 - insect screen	"	0.640	No	0.708
" " "	"	"	Yes	0.648

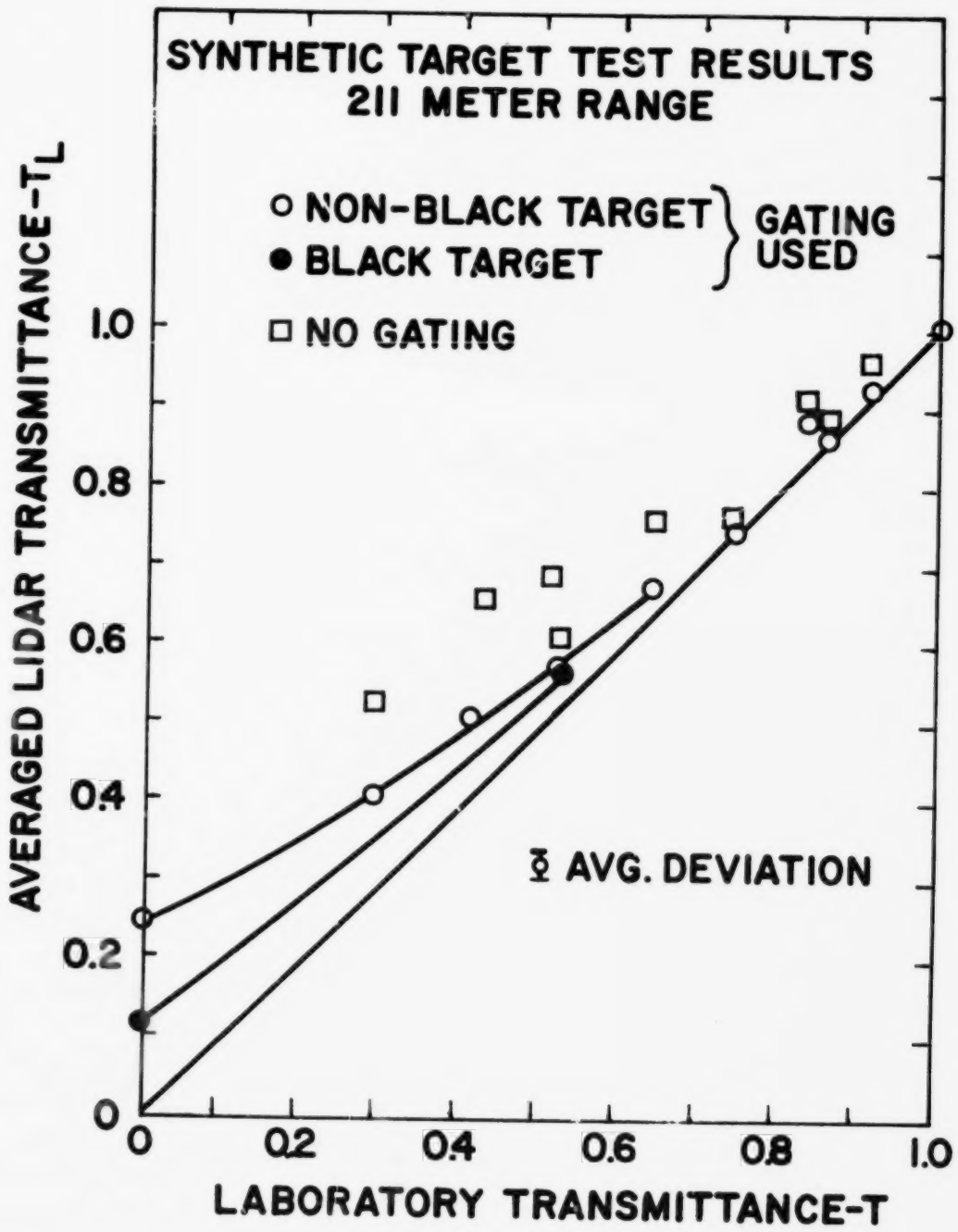

Figure 3.7 Averaged lidar determined target transmittance T_L, vs. laboratory determined transmittance, T, with and without off-gating at 211 meters range.

decreasing target reflectance to a minimum. Since the unblackened targets were either white or bright aluminum, the two curves shown probably represent upper and lower bounds on the lidar system's measurement error for the range $0 \leq T \leq 0.6$.

The remaining open circle data points lie generally along the line of perfect agreement and are for the specularly reflecting glass and plexiglass targets where afterpulsing should not have occurred. An exception is the double plexiglass target result ($T = 0.837$) which clearly falls above the line. In the case of both plexiglass target configurations ($T = 0.837$ and $T = 0.915$), off-gating yielded a definite decrease in system error. Afterpulsing is clearly visible, although small, on the oscillograms corresponding to the double plexiglass target measurements although it cannot be seen on the single target oscillograms. The only explanation here is that the plexiglass was cleaned repeatedly with Windex and a soft cloth, and may have become sufficiently scratched to have a diffuse component of reflectivity giving rise to the error.

Before discussing the similar plot of test results for the 319 meter range it is instructive to look at Figure 3.8 which shows a lidar shot through the clear single target holder aperture ($T = 1.00$) similar to that shown in Figure 3.4 for 211 meters range. It is clear from the plot that the system exhibited $1/r^2$ performance for extended ranges on both sides of the target holder. However, the measured transmittance was 0.961 as opposed to unity. Further, it can be seen that a deviation from $1/r^2$ performance occurred just before the target range. This all points out what, in retrospect, was a poor choice of target location.

The target holder was placed approximately 10 meters from the edge of a building roof on a large flat portion of the roof that extended for more than 100 meters beyond the target; that is, the target range occurred just beyond a sharp discontinuity in the terrain. Prior to the roof edge the optical path was up to 60 feet above a parking lot while once beyond the roof edge it was only a few feet from the roof top. Although the effect is in the right direction and although it was a bright sunny day, an unreasonably large temperature increase over the roof is required ($\sim 45^{\circ}$F) to explain the drop in scattering signal.

Close examination of the original oscillogram reveals the presence of a sharp signal spike of about 1.4 cm amplitude relative to the ambient signal precisely at the target range (4.6 cm from the start of the sweep). Clearly some of the beam was intercepted by the black target holder. However, interception of the entire beam by the black felt target yielded a signal more than 200 times the ambient atmospheric scattering level (it produced saturated photomultiplier tube output of approximately 20 volts, thus the light scattering may have been much more than 200 times greater) while this interception provided an additional signal level only 0.7 times the ambient level. Thus the resulting beam energy loss through the aperture must have been less than 0.5 percent yielding a minimum transmittance of T = 0.995. A more likely explanation for $T_L < 1.0$ is that the building roof acted as a poor source or a better sink for particulate aerosols than the parking lot, causing a drop in light scattering over the roof.

Figure 3.9 shows the results of the synthetic target tests at 319 meters. Had it not been for the clear aperture result discussed above, the data would look quite good and consistent with those shown in Figure 3.7. Again the

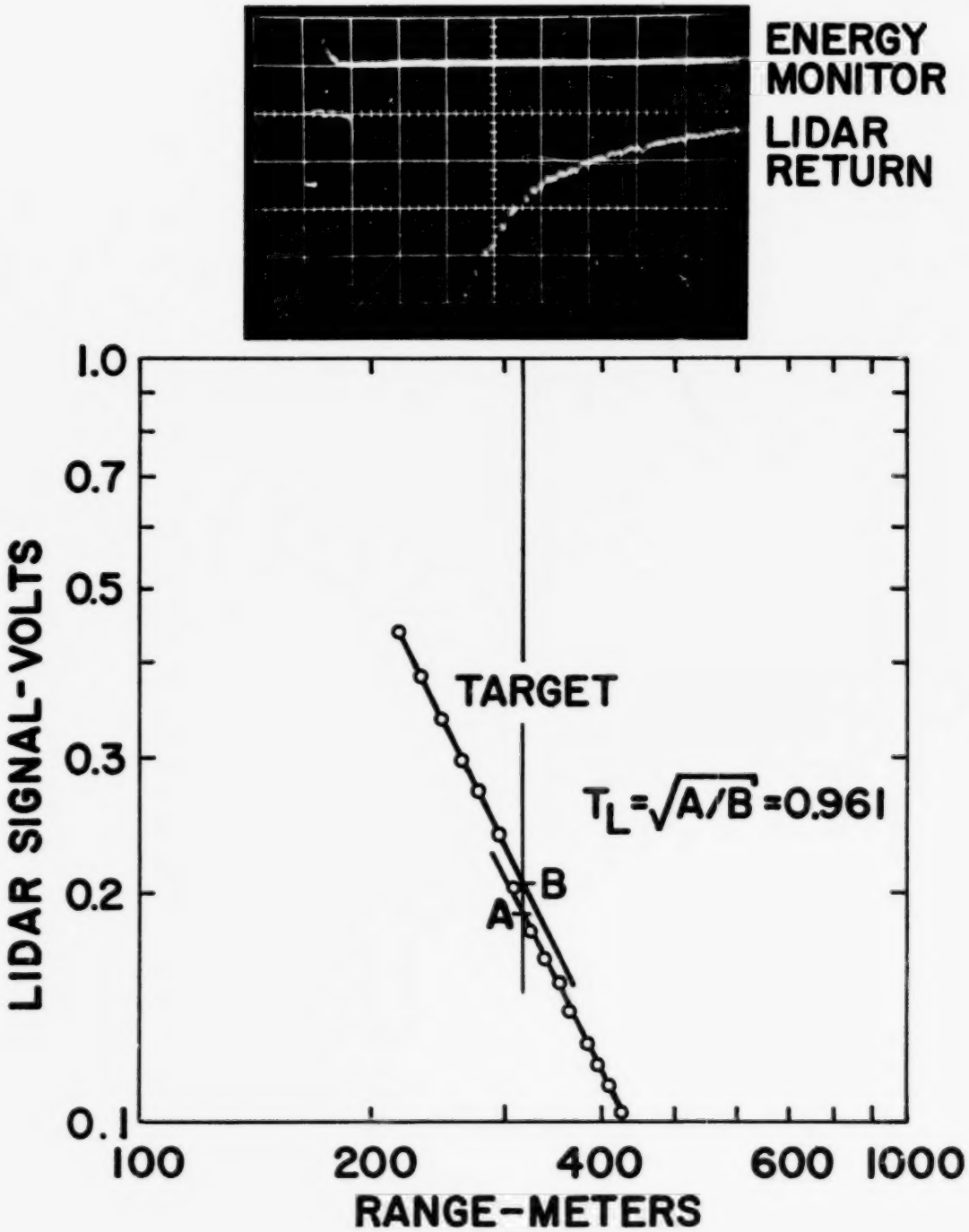

Figure 3.8 Lidar shot through the clear target aperture (T = 1.00) at 319 meters range.

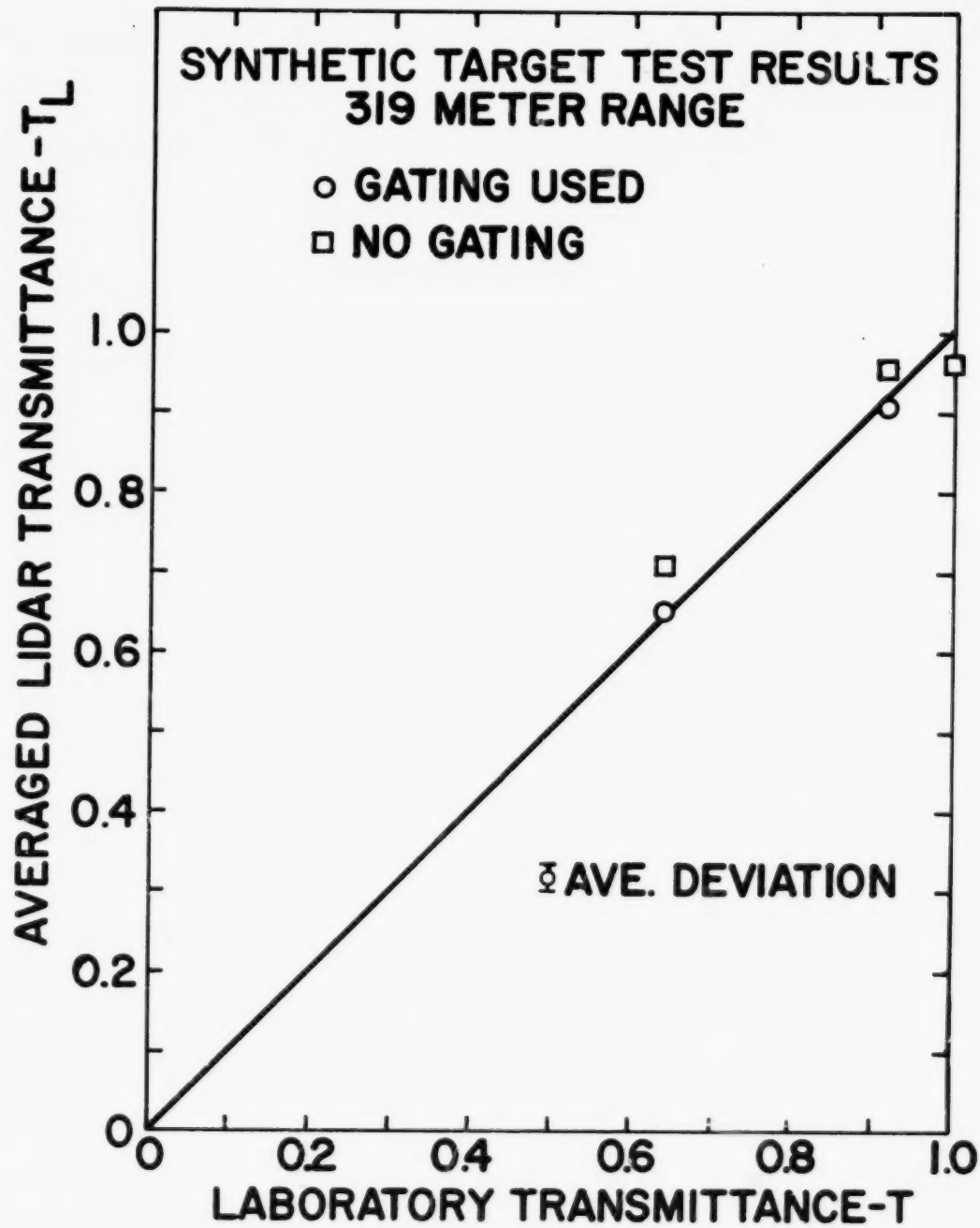

Figure 3.9 Averaged lidar determined target transmittance, T_L, vs. laboratory determined transmittance, T, with and without off-gating at 319 meters range.

plexiglass target data (T = 0.915) shows an improvement through off-gating although no visible afterpulsing appears on the oscillograms, while the single insect screen target (T = 0.645) result shows an expected improvement through off-gating with visible afterpulsing on the oscillograms. It is hard to say to what extent the "roof effect" influenced the target results. All of these data were taken on one afternoon within a period of about 1 1/2 hours and it is tempting to simply "correct" the results by dividing through by 0.961. However, since only one clear aperture oscillogram was taken, it is difficult to be sure that this effect remained constant throughout the test period. It seems best to simply accept the additional error and rely on the 211 meter range results to give the best indication of system capability and accuracy.

4. FIELD TESTS ON REAL SMOKE PLUMES

4.1 Local Field Tests

Two separate local field tests were made at Philadelphia Electric Company power stations near the General Electric Valley Forge Space Center. The first tests were made shortly after completion of the equipment in April 1971 for the purpose of initial checkout of the system using a real plume. This was done with the cooperation of the Philadelphia Electric Company at their Barbadoes Island power station near Norristown, Pa. The site is shown in Figure 1.1. The equipment was operated, without difficulty, for several hours while shots were taken through both an oil fired and a coal fired plume. Much of the time was spent assessing system operation and alignment as well as determining the effect of varying the off-gating pulse width in search of an optimum value for real plumes and as a result not much real transmittance data was obtained. Only a few oscillograms were reduced indicating a transmittance of approximately 0.65 for the coal fired plume and nearly unity for the essentially invisible oil fired plume.

A second field test, in which Mr. W. D. Conner and Mr. N. White of EPA participated, was made on 8/26/71 at the Cromby Station of PECO near Phoenixville, Pa. Two stacks were available, again one coal fired and the other oil fired. The coal fired plume was clearly visible against a blue sky and visual judgement by those present brought an estimate of less than 0.50 transmittance The oil fired plume was visible only through the refractive effects of the hot gases. The lidar system was fired through both plumes both with and without photomulti-

plier tube off-gating. The results of these measurements are shown in Table 4.1 below.

Table 4.1 - Local Field Test Results Cromby Station - Philadelphia Electric Co.

Type of Stack	Oscillogram No.	Trans-mittance	Gating	Range
Oil Fired	8/26/71-3	0.930	No	225 m
Oil Fired	8/26/71-4	0.956	Yes	225 m
Oil Fired	8/26/71-5	1.000	Yes	225 m
Oil Fired	8/26/71-6	0.915	No	225 m
Coal Fired	8/26/71-8	0.369	No	210 m
Coal Fired	8/26/71-12	0.148	Yes	210 m

No afterpulsing was observed for the lidar shots through the oil fired plume, and probably the gated and non-gated shots are equally valid measures of the plume's transmittance. The variation in transmittance was probably real and related to the periodic rapping of precipitators to dislodge collected particulate matter. Some of this dislodged material goes up the stack and, on denser plumes, can be seen as dark puffs of smoke. On the other hand, strong afterpulsing was observed on the lidar returns from the coal fired plume. Comparison of the gated and non-gated results shows the usual large improvement in system performance when gating was used. Because of the reduced accuracy of the measurement at these low transmittance values (as shown in Figure 3.7), the value of $T_L = 0.148$ can only be regarded as an upper bound for the real value. It was clear from this measurement that visual plume appearance was not strongly correllated with plume transmittance or opacity.

4.2 Field Tests in Western Pennsylvania and West Virginia

Following the lidar evaluation using synthetic targets, the system was taken on a 3 day field trip to West Virginia and western Pennsylvania. Specific test sites had been previously selected by Mr. W. D. Conner of EPA with the cooperation of the Allegheny Power and Light Co. The three sites selected were all coal burning power stations and were specifically the Albright Station at Albright, West Virginia, the Fort Martin Station near Point Marion, Pa., and the Western Penn Station in Springdale, Pa.

Two of the sites selected, Albright and Western Penn, had stacks situated in valleys in such a way that telephotometer plume transmittance measurements could be made simultaneously with the lidar measurements. The telephotometer technique for plume transmittance measurements is described in detail in reference 1 and is best understood by examining Figure 4.1

Plume-to-sky contrast can be obtained for any plume regardless of plume-hill-sky geometry simply by a comparison of the luminance of the sky through and directly adjacent to the plume and is given by

$$C = (I_s - I_{sp})/I_s \tag{4.1}$$

where I_s is the sky luminance and I_{sp} is the apparent sky luminance seen through the plume. I_{sp} will be the sky luminance attenuated by the transmittance of the plume plus the luminance of the plume itself due to the scattering of ambient light by the plume. It is this latter component that disallows plume-to-sky contrast from being a good measure of plume transmittance or opacity.

In order to remove this variable plume luminance factor, it is necessary

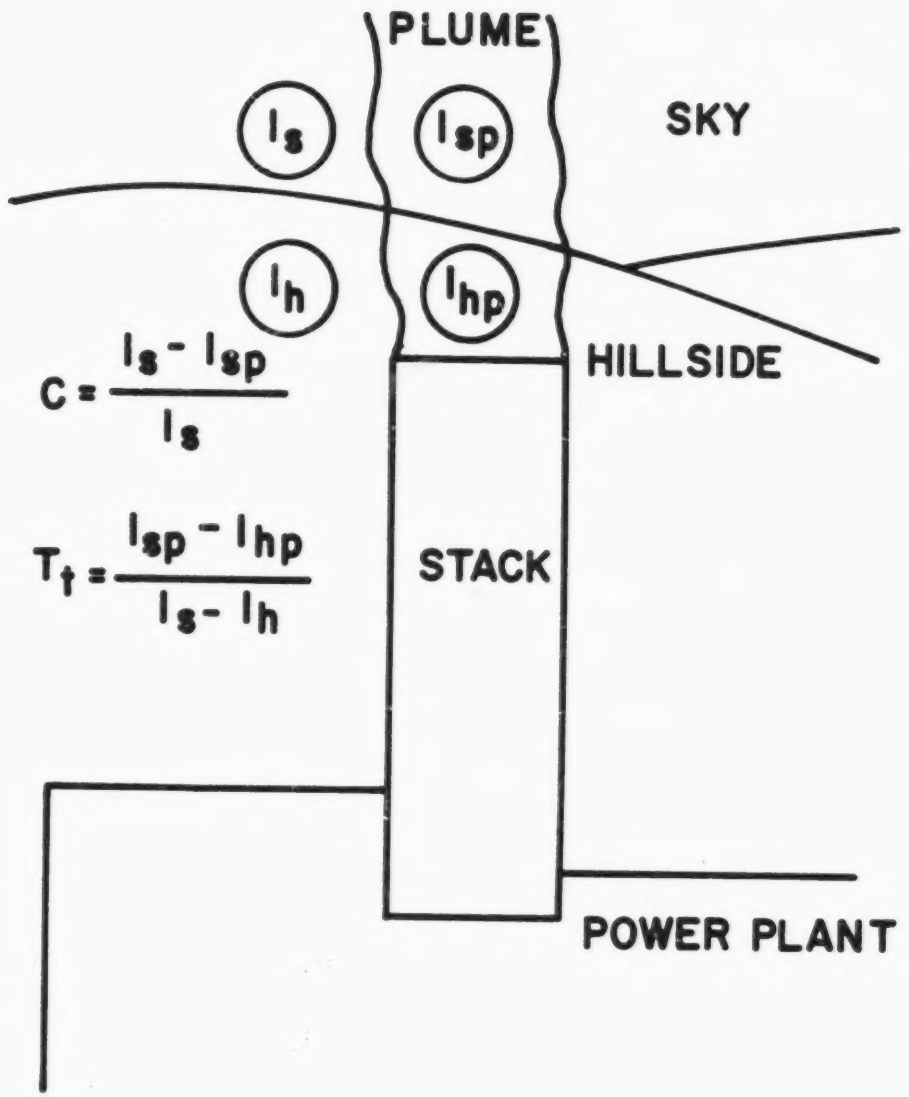

Figure 4.1 The telephotometer technique of measuring plume-to-sky contrast, C, and plume transmittance, T_t, by comparison of the luminance of the circled areas shown.

to arrange the geometrical situation shown in Figure 4.1 where the change in luminance of two separate backgrounds (sky and hill) caused by the plume can be compared and the effect of plume-scattered ambient light can be factored out. In this situation the plume transmittance is given by

$$T_t = (I_{sp} - I_{hp})/(I_s - I_h) \qquad (4.2)$$

where I_{sp} and I_s are as previously defined, I_h is the luminance of the hillside viewed adjacent to the plume and I_{hp} is the apparent hillside luminance seen through the plume.

In actual practice the measurements were made with a portable, battery operated, narrow field telephotometer using a red filter with a mean response of 6510 A in order to correspond with the 6943 A lidar measurement. It was not possible or desirable to locate the telephotometer and the lidar in the same exact spot since the telephotometer had to have its optical path terminating on a hillside while this was to be avoided with the lidar from a safety point of view. The relative viewing angle between the two instruments never exceeded 10 degrees, however restricting the variation in plume path length for the two measurements to less than 1.5 percent.

4.2.1 Tests at Albright, West Virginia

The first site visited was the Albright Station on 9/18/71. This site had been selected because of geometry allowing the telephotometer transmittance measurement to be made in addition to the high velocity of its plumes which yielded a large distance of vertically rising, well defined plume structure. It was known to be an older plant than some and to have fairly low transmittance plumes.

On arriving at the plant, a discussion was held with the local management at which point they agreed to reduce the load on the plant in an attempt to increase the transmittance of the plume.

The test site is shown in Figure 4.2. These photographs were taken at different times during the day under quite different lighting conditions although the telephotometer measurements indicated a relatively constant transmittance of about 10 percent. This illustrates the lack of correlation between visual plume appearance (plume-to-sky contrast) and plume transmittance or opacity. It is interesting to note that although the plumes are not dark in Figure 4.2a, the left hand plume totally obscures the far hillside.

A series of lidar and telephotometer measurements were made on both the number 2 (center) and the number 3 (right hand) plumes throughout the afternoon. The lidar measurements were made at a range of 300 meters. The results of these measurements are shown in Figure 4.3 as plume transmittance, both lidar-determined (T_L) and telephotometer-determined (T_t), as well as telephotometer-determined plume-to-sky contrast (C) vs. observation time and power plant stack operating load. The amount of useful lidar data was limited by occasional rain and some experimenting with operating without gating in addition to system alignment checks. The telephotometer transmittance data shows an average transmittance of about 8 percent on both the number 2 and 3 stacks prior to the load reduction on the number 3 stack. The oscillations shown in this data are real and usually represent the effect of rapping the precipitators. The time required for the series of four measurements needed to determine transmittance by telephotometry was approximately 5 seconds, and short enough to measure the variations.

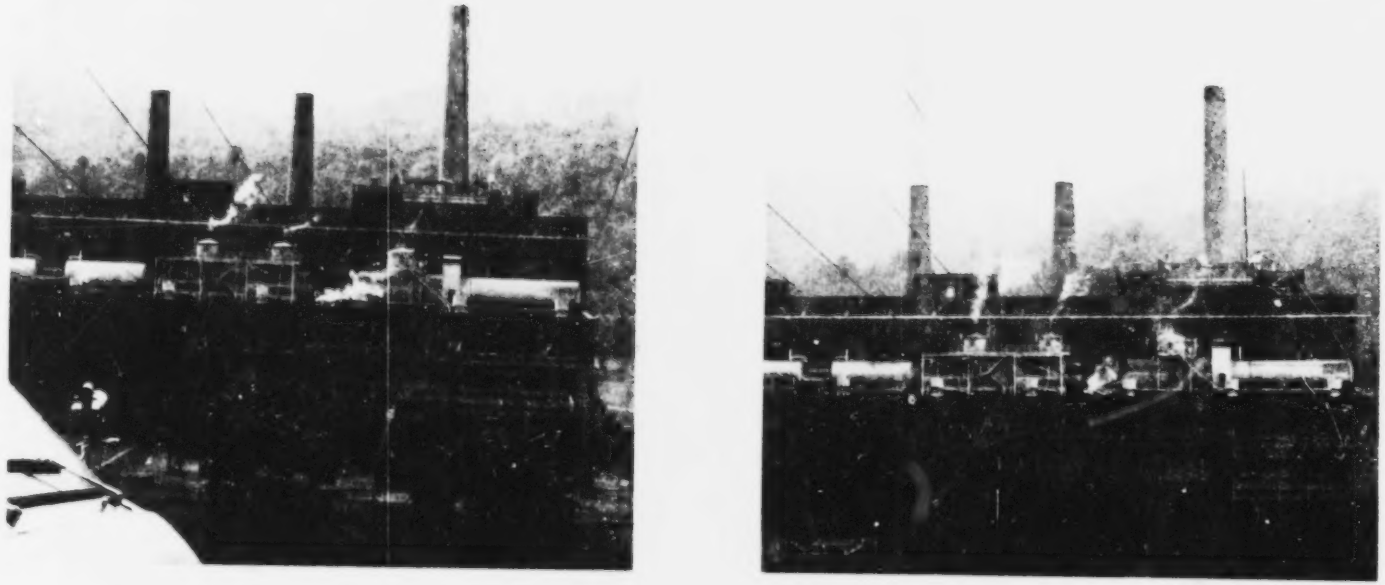

(a) (b)

Figure 4.2 Two photographs (a and b) of the Albright Station of the Allegheny Power and Light Co., Albright, West Virginia. The right hand photograph (b) was taken with much more overcast lighting conditions than (a) although telephotometer measurements indicated a relatively constant transmittance of about 10 percent. The telephotometer and lidar truck are shown in the foreground in (a). This illustrates the lack of correlation between visual plume appearance (plume-to-sky contrast) and transmittance or opacity. Note that the hillside is totally obscured by the left hand plume.

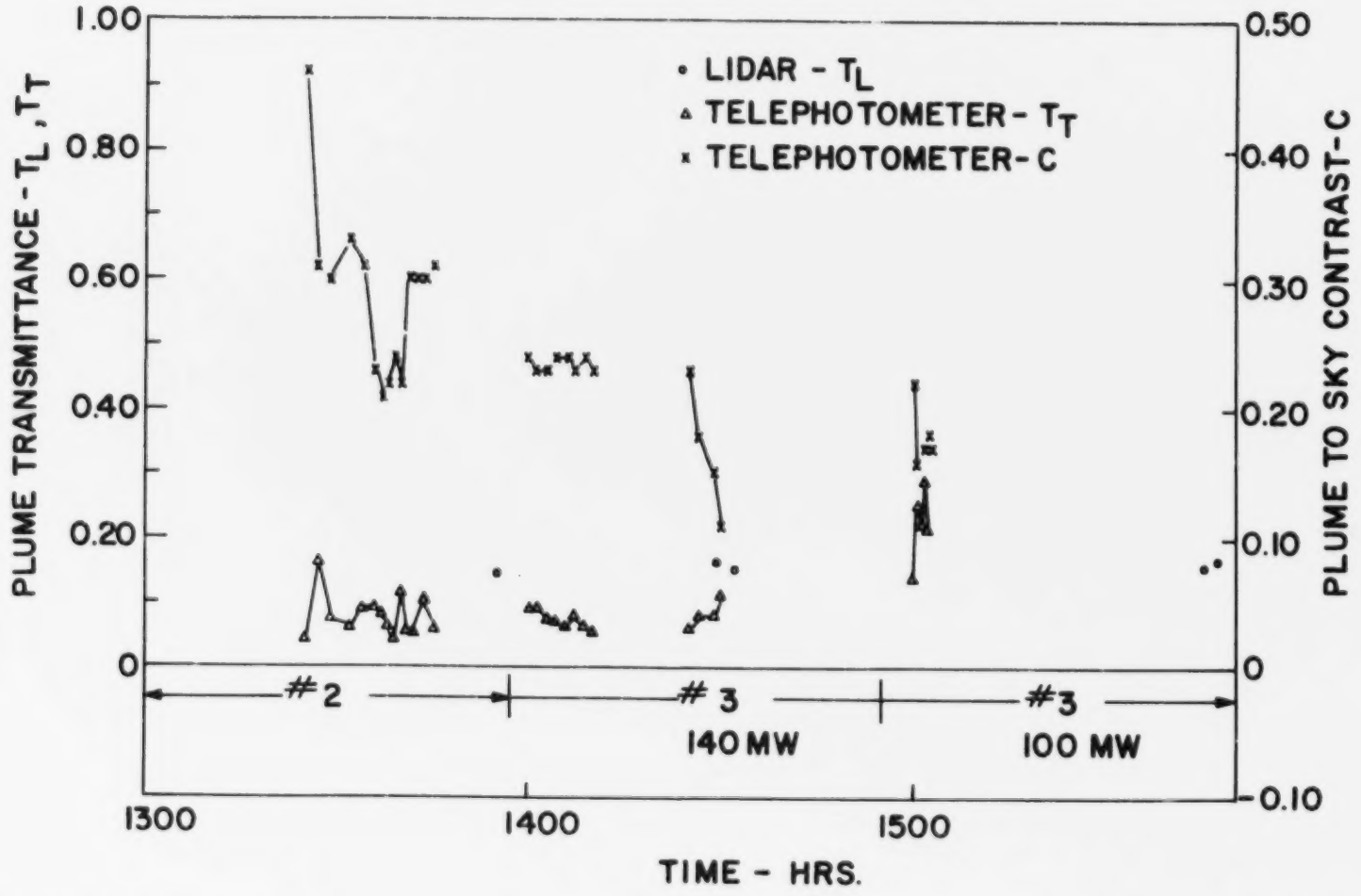

Figure 4.3 Lidar and telephotometer determined plume transmittance plus plume-to-sky contrast vs. observation time and power plant stack operating load. Data taken at the Albright Station, Allegheny Power and Light Co., Albright, West Virginia, 9/18/71.

Lidar data during this period shows a transmittance of 15 to 17 percent and must be considered an upper bound measurement since severe afterpulsing was present and the laser pulse could be seen visually on the plume through the 10 power rifle scope. This is not surprising when the synthetic target results shown in Figure 3.7 are compared with these results. The target tests would predict a lidar-determined transmittance of from 16 to 27 percent for an 8 percent transmitting target depending on its reflectivity. This implies a low reflectivity for the plume although it certainly was not as low as the black felt target on which the lidar pulse was invisible.

At about 1500 hours the load was changed on the number 3 stack from 140 MW to 100 MW. The telephotometer data show an average increase in transmittance to greater than 20 percent, while the lidar data, taken only at the very end of the period because of intervening rain, show only a slight increase in transmittance. There is too little data and temporal correlation to conclude anything from these results.

Finally, it can be seen that plume-to-sky contrast (C) varies widely during periods of relatively constant plume transmittance as shown pictorially in Figure 4.2. This wide variation in contrast was due to wide variation in ambient illumination of the plumes resulting from uneven overcast sky conditions.

4.2.2 Tests at Point Marion, Pennsylvania

The lidar system was driven to the Fort Martin Station, Allegheny Power and Light Co. near Point Marion, Pennsylvania for the second day of testing on 9/19/71. Again the weather was overcast and rain threatened. It was not

possible to arrange to make telephotometer transmittance measurements at this site although plume-to-sky contrast measurements were made with the telephotometer sitting next to the lidar system. This site was chosen as representing one of the most modern coal burning power stations available with a relatively clean plume from each of its two stacks. Again the local management was consulted and as had been prearranged, they agreed to vary the load on each of the two stacks in an attempt to vary the transmittance.

A sample of the lidar data and results is shown in Figure 4.4. Here the shot is through the number 2 plume operating at 535 MW and at a range of 487 meters. The oscillogram and the reduced data plot look similar to those obtained with the synthetic targets shown in Section 2. Good $1/r^2$ performance is evident on both sides of the plume and no afterpulsing is visible. The computed transmittance is unambiguous and is supported by the near invisibility of the plume.

A majority of the data taken at this site looked this good (Figure 4.4) but, in a limited number of cases, lack of $1/r^2$ performance was observed on the far side of the plume. These cases showed steeper than $1/r^2$ dependence and occurred in the absence of any visible afterpulsing. It has been concluded that this must be the result of thermal lensing due to the hot plume gases. Limited attempts at a rough analysis of the problem have not yielded a simple optical configuration from which numerical results can be obtained. This is particularly true when the plume is turbulent and its optical properties vary widely from place to place and with time. Thus, all that can be said at this point is that the problem occasionally exists, it can be readily recognized and by weighting most heavily

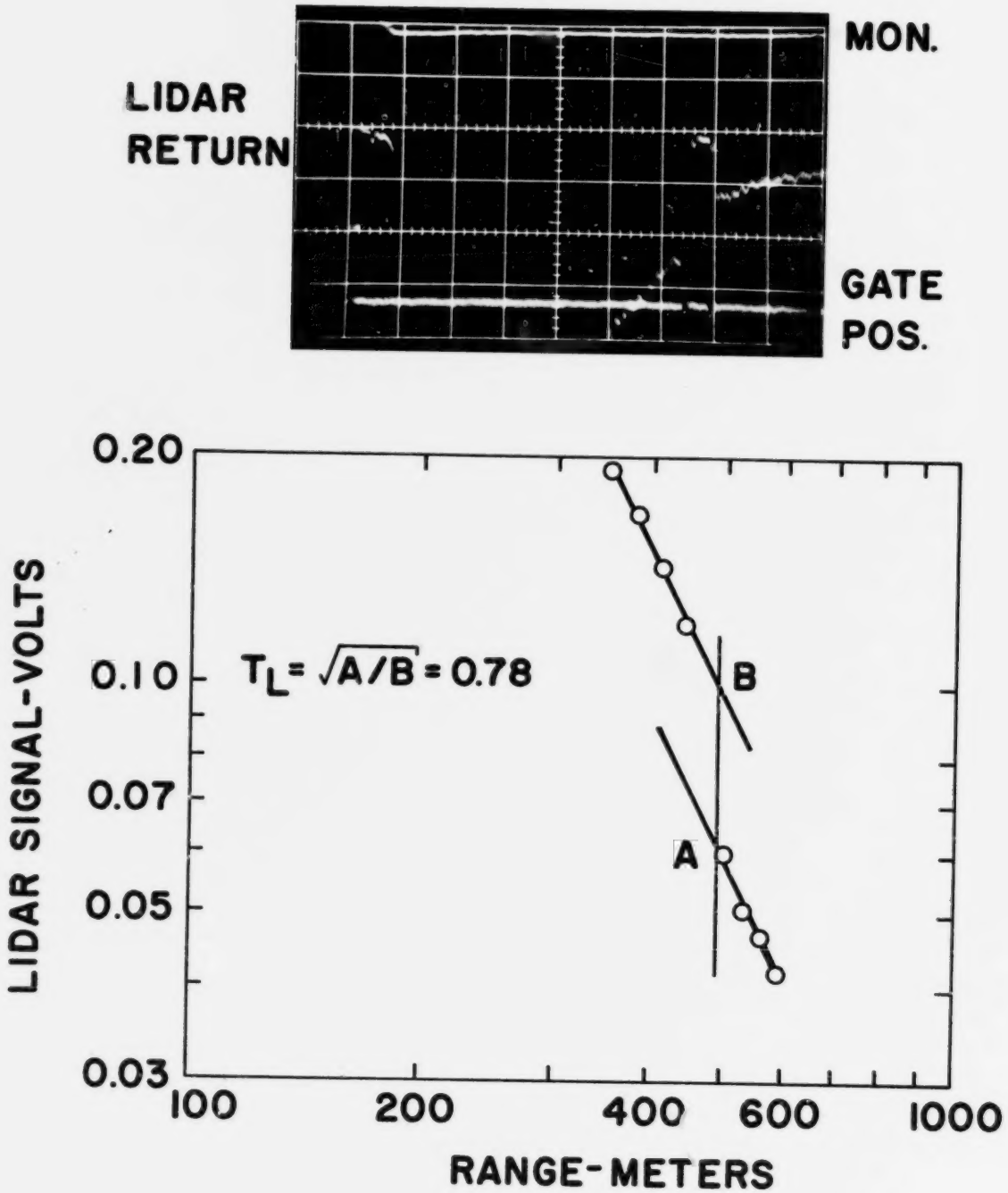

Figure 4.4 Lidar shot through a power station plume; Fort Martin Station, Allegheny Power and Light Co., Point Marion, Pennsylvania, 9/19/71. This is a coal fired plume operating at 535 MW with a lidar range of 487 meters.

those points nearest the plume, its effect can be minimized. This effect had not been noticed on previous real smoke plume results, but experience with high transmittance plumes had been limited and early afterpulsing on low transmittance plumes masked the effect if and when it occurred.

The results of the lidar and telephotometer measurements can be seen in Figure 4.5 which is similar to Figure 4.3 in format. Here there are no telephotometer transmittance measurements to compare the lidar results with, but some interesting observations can still be made. The first set of measurements were made on the number 2 stack plume operating at 535 MW. This plume was nearly invisible as indicated by the low plume-to-sky contrast shown. The lidar-determined transmittance oscillated around 0.80, a transmittance level where the measurement error is vanishingly small according to the synthetic target test results. The second measurement period was devoted to the number 1 stack plume operating at 480 MW. This plume was clearly visible, as the higher values of plume-to-sky contrast indicate. The lidar-determined transmittance of about 0.40 is an upper bound since afterpulsing was present on the oscillograms. The synthetic target test results of Figure 3.7 indicate the real transmittance should have been in the range of 0.30 to 0.40.

Following a lunch break the load was alternately changed on both stacks. First the load on the number 2 stack was dropped to 380 MW. Intermittant rain showers and the existence of uncooperative cooling tower plumes allowed only two good lidar shots but they indicate an increase in transmittance to about 0.92. No telephotometer data was taken during this period. The final data series was taken using the number 1 plume at the reduced load of 400 MW. This series

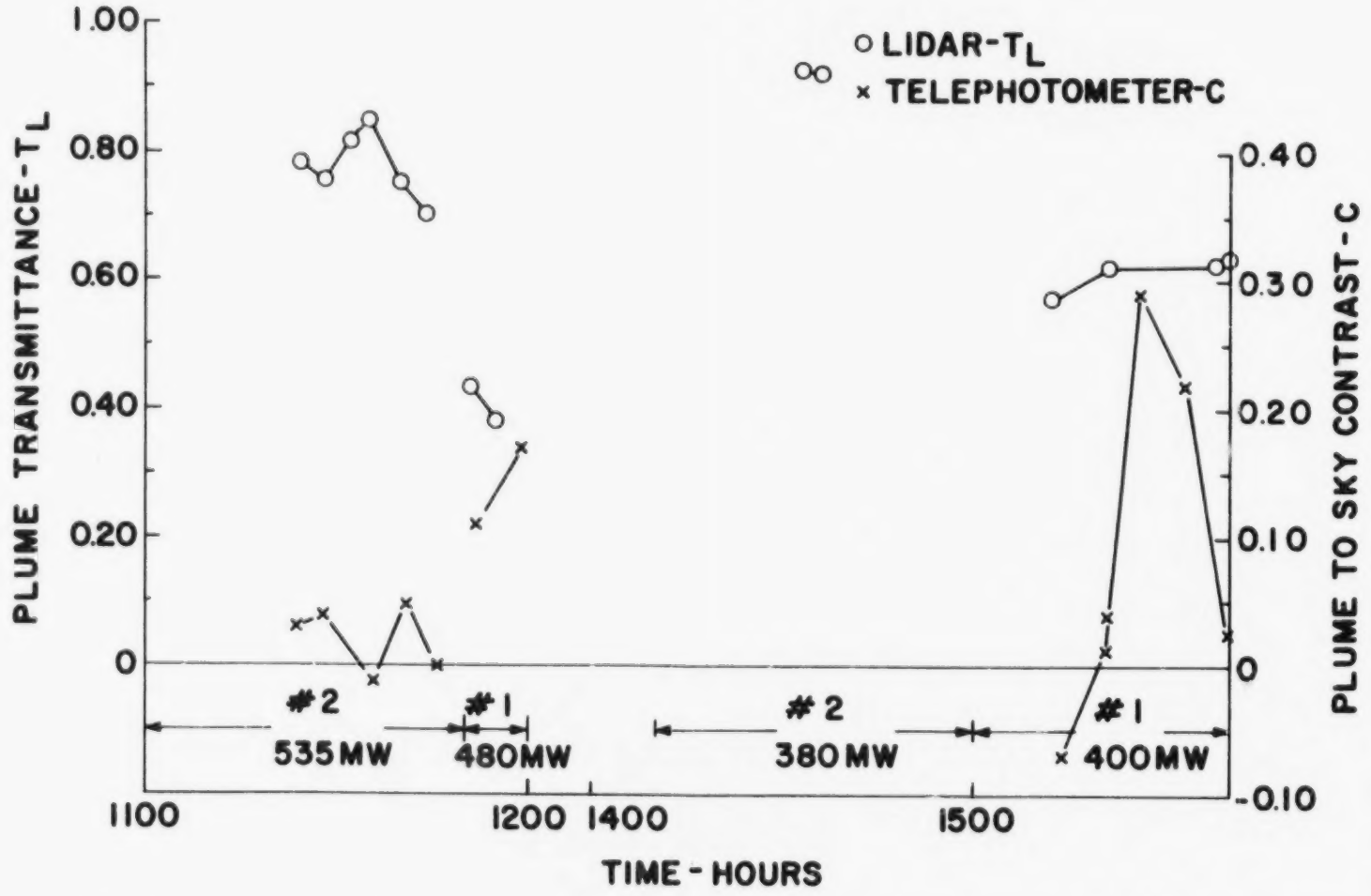

Figure 4.5 Lidar-determined plume transmittance and telephotometer determined plume-to-sky contrast vs. observation time and power plant stack operating load. Data taken at Fort Martin Station, Allegheny Power and Light Co., Point Marion, Pennsylvania, 9/19/71.

is the best example of the lack of correlation between plume-to-sky contrast and plume transmittance. Here the transmittance rose to about 0.60 from 0.40 due to the load reduction and was relatively constant, while the plume-to-sky contrast varied from -7 percent to nearly + 30 percent due to wide lighting changes.

4.2.3 Tests at Springdale, Pennsylvania

On the final day of the field trip, 9/20/71, the lidar system was taken to the Western Penn Station of the Allegheny Power and Light Co. at Springdale, Pa. This site was chosen because of suitable hill-plume geometry for the telephotometer measurement and because at least one of the plumes was relatively clean (in fact nearly invisible except for refractive effects). This one plume was used for all of the data and the load was not varied during the day. Again the weather was quite overcast with occasional short rain showers until about 1500 hours when a steady rain halted the operation.

The results of this testing are shown in Figure 4.6, again with lidar and telephotometer-determined plume transmittance as well as telephotometer-determined plume-to-sky contrast plotted vs. observation time. This data was taken at a range of 390 meters. One feature, in addition to the weather, limited the amount of data taking. A small smelting plant with a broad, diffuse smoke plume was located directly up wind of the power plant. This plume occasionally enveloped the top or near side of the stack being observed, interfering with the measurement. This was easiest to spot from the lidar traces which showed large discontinuous returns at ranges other than the stack range and these traces were discarded.

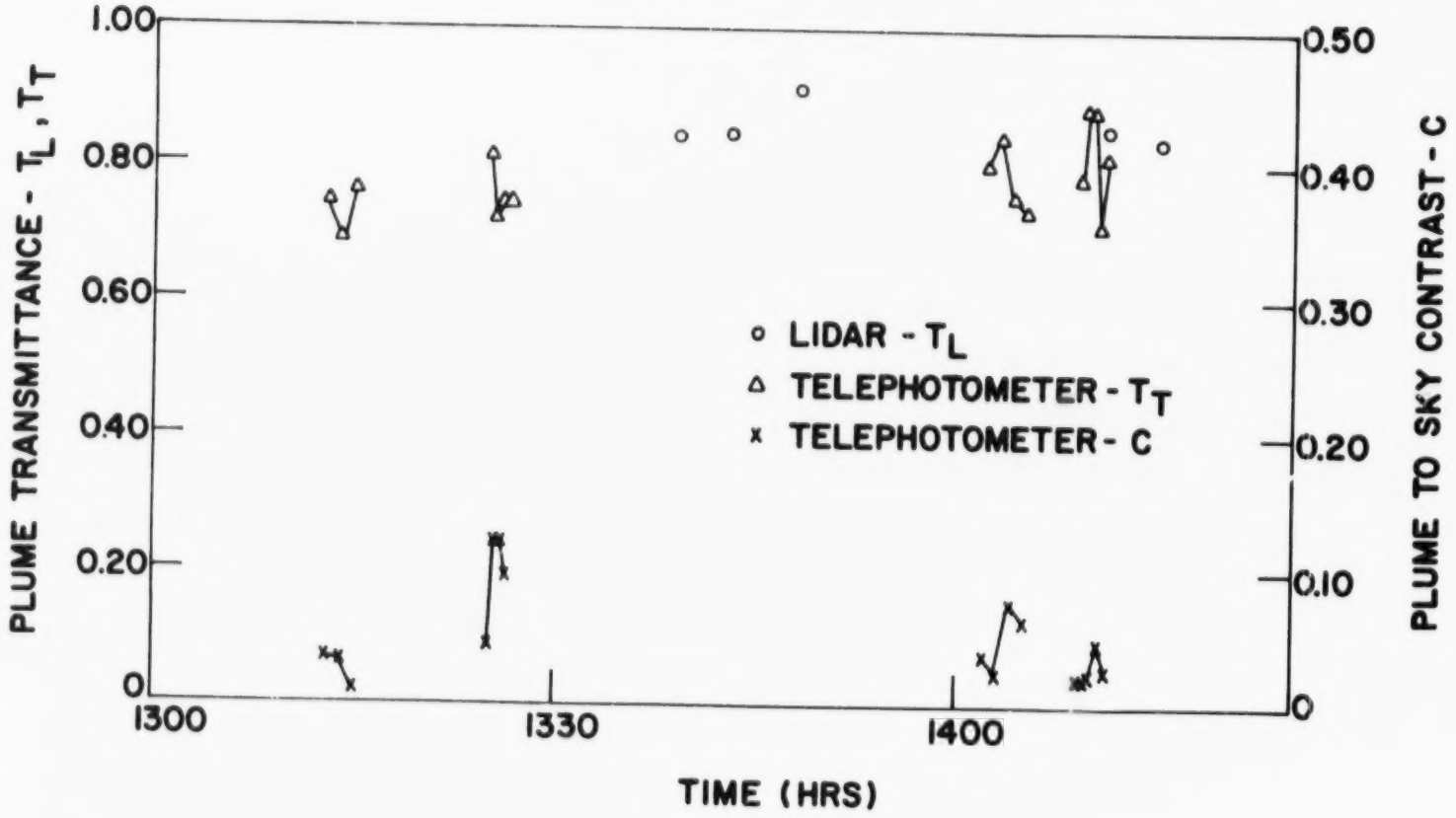

Figure 4.6 Lidar and telephotometer-determined plume transmittance and telephotometer-determined plume-to-sky contrast vs. observation time. Data taken at the Western Penn Station, Allegheny Power and Light Co., Springdale, Pennsylvania, 9/20/71.

The data show good general agreement between the two transmittance measuring techniques, especially in the last series of measurements where there is reasonable temporal overlap. Again, the plume transmittance was high enough that the lidar error should have been negligible. Since the ambient lighting conditions did not vary much, the day remaining generally overcast, plume-to-sky contrast did not show much variation and was low verifying the low plume visibility.

Finally, it should be mentioned that lack of $1/r^2$ performance on the far side of the plume occurred for the last three of the five lidar data points shown. As has been discussed in the preceding section, this is believed to be due to thermal lensing by the hot plume gases causing some of the lidar pulse to diverge beyond the field of view of the receiving system. (It is implicit in this argument that the field of view of the receiver is much larger than the laser divergence such that the two see different mean portions of the plume's thermal lens and thus differential focussing is possible). Again, the closest in far side data points were used for obtaining the transmittance, T_L, in an attempt to minimize this effect. This generally meant a point 40 meters down range of the plume. If, on the other hand, data points 100 meters down range had been weighted most heavily the computed transmittance values would have been lower by less than 10 percent. It is, of course, not proven whether the thermal lensing hypothesis is correct or whether random inhomogenieties in the atmospheric scattering caused this lack of $1/r^2$ performance. The evidence is strong, however, for thermal lensing since in all cases the signal falls off monotonically and faster than $1/r^2$, while with

atmospheric variations this should be random. Further, the lack of $1/r^2$ performance is always observed on the far side of the plume. Finally, it is clear that it is not an inherent characteristic of the lidar system since the majority of such plume shots and all of the synthetic target test shots where afterpulsing did not occur show good far side $1/r^2$ performance.

5. CONCLUSIONS

During the construction and evaluation of the lidar system it was used extensively under field operating conditions. It was driven over 1000 miles in its present configuration on a variety of road surfaces and operated in a wide variety of temperature and relative humidity conditions. The system performed satisfactorily through all of this requiring little or no maintenance. Optical alignment was stable and electronics performance was reliable. The physical arrangement in the truck proved to be quite convenient and the pointing capability and azimuth and elevation limits were more than sufficient. It is estimated that once familiarity has been gained with the equipment, it is possible to begin data taking within 15-20 minutes after having arrived at a test site. This time could probably be shortened to 5 minutes or less by employing all solid state electronics (eliminating warm-up) and by providing motor generators that did not have to be removed from the vehicle.

Some observations can be made relative to the measurement of real smoke plumes. It is generally necessary to use a minimum off-gating pulse width of 200 nanoseconds with 250 and even 300 nanoseconds being commonly used. Plume ranges varied from just over 200 meters to just under 500 meters and were dictated by accessibility of the site to the vehicle, wind direction and strength, the existence of cooling tower plumes, multiple power plant plumes, and the desire to reduce the elevation angle as much as possible so that the lidar optical axis intersected the plume close to perpendicularly. These ranges mentioned do not represent system limits. The minimum range limit with the lidar

axes aligned at infinity is about 150 meters (closer if lidar alignment is changed) while the maximum range depends on the transmittance of the plume being measured and the atmosphere backscattering. However, taking the data shown in Figure 4.4 as an example, it probably would have been possible to have made this measurement of a fairly high transmittance plume (T_L = 0.78) at more than twice the range or nearly 1000 meters based on the signal levels and system noise.

The accuracy with which the lidar system can remotely measure transmittance or opacity is best seen on Figures 3.7 and 3.9, the synthetic target test results. Although these were thin synthetic targets, their transmittance was well known and constant which was not the case for the telephotometer measurements on real plumes. Since that data shown is averaged over a number of lidar shots for each point such random error sources as oscillogram reading, atmospheric inhomogeniety, and lidar alignment and aiming should have been averaged out. This leaves only the systematic error or system inaccuracy caused by afterpulsing which depends on target reflectance and is shown on Figure 3.7 by the amount that the curved lines deviate from the line of perfect agreement. The following general statements can be made about the maximum measurement error in lidar determined transmittance, T_L, assuming maximum target reflectance:

A. The error in T_L is always positive, such that T_L is always an upper bound transmittance.

B. The error in T_L is less than + 12 percent for T greater than 0.50.

C. The error in T_L is less than + 2.5 percent for T greater than 0.80.

In the previous section a comparison was made between the lidar and tele-

photometer measured transmittance values during the field tests on real smoke plumes. In general, the lidar measurements agreed with the telephotometer measurements. Due to bad weather conditions, there is not as much data and data overlap as desired but agreement between the two techniques is still evident, particularly at the Western Penn Station in Springdale where plume transmittance was high and the lidar could be expected to yield good results. Again, the measurements made at Albright Station, showing telephotometer determined transmittances of about 8 percent with lidar determined transmittances of about 15 to 17 percent, agree well with what is expected of the lidar system from the synthetic target test results at these low transmittance levels.

Finally, it is clear that, in general, plume-to-sky contrast (plume visibility) is unrelated to plume transmittance. Plume-to-sky contrast depends not only on the transmittance of the plume (the amount that the plume attenuates the luminance of the sky seen through the plume) but also on the direct scattering of sunlight by the plume. Thus, plume-to-sky contrast is quite dependent on ambient lighting conditions while plume transmittance is not.

6. RECOMMENDATIONS

After having used the mobile lidar system extensively, some desirable system modifications have become apparent. The reasons for these modifications along with proposed solutions are discussed in the following paragraphs.

Since the lidar signal return, for a homogeneous scattering atmosphere, behaves inherently as $1/r^2$, it is necessary to transfer the data from a polaroid oscillogram to a double logarithmic plot to make the necessary linear extrapolations prior to computing the far side to near side signal ratio, A/B. This is a time consuming process done with dividers and can take 20 to 30 minutes for one oscillogram before the results are known. If the signal were not $1/r^2$ in nature but constant with range, the data reduction could be done directly on the oscillogram taking the ratio of the average signal level before and after the plume. It is possible to add an amplifier to the system, following the photomultiplier tube and in front of the oscilloscope preamplifier, whose gain is proportional to time squared and thus, range squared. This would have the effect of cancelling the $1/r^2$ signal dependence yielding an output constant with time (range) for a homogeneous scattering atmosphere. The design of such an amplifier has been considered in some detail and appears quite feasible. It could have a 3.5×10^6 Hz frequency response with acceptable noise and would operate over a range of from 100 to 500 meters. The amplifier would be physically small, consume negligible power and could be bypassed by flipping a switch, leaving the system in its original configuration. This type of r^2 compensation would be universally applicable to any photomultiplier detector design used with the system and would not require re-working the photomultiplier tube

and power supply circuitry or involve the necessary photomultiplier tube circuit design compromises which are required when considering varying the gain of the tube to accomplish the r^2 correction while preserving linear tube response over the wide signal dynamic range encountered.

A second desirable modification would be the elimination of afterpulsing, thus eliminating the dominant source of error in the lidar measurement. Much effort has been expended already, as outlined in Sections 2 and 3 and detailed in Appendix B, on photomultiplier tube gating without success in the elimination of afterpulsing. This has led to a clearer understanding of the afterpulsing mechanism as well as the magnitude of the effect of afterpulsing on transmittance measurement error. As a result, two separate solutions to the problem have emerged. Of the two, one would be simplest to implement requiring few basic system changes but would be less assured of success, while the other would require optical and mechanical modifications to the receiving system but should reduce afterpulsing effects to a negligible level.

The first solution mentioned consists of purchasing a recently available photomultiplier tube commercially made with an internal screen grid adjacent to the photocathode. This gating option has not previously been available and most certainly will stop afterpulsing. The question is whether the applied electric field will be sufficiently uniform that charge redistribution on the photocathode will not take place avoiding damaging the tube's on-response following realistic off-gating pulse durations. If necessary, with this new type of tube steps could be taken to prevent charge redistribution on the photocathode. This solution should probably be tried first since it is the easiest to implement and would involve the least

system modification.

The second solution involves placing a fast optical shutter in front of the photomultiplier tube, disallowing the troublesome plume return pulse from ever getting to the photocathode. This can be done using a Pockel cell shutter and would employ the current photomultiplier tube. In principle, this technique should nearly eliminate afterpulsing but it was not seriously considered prior to this because of cost, complexity and the difficulty of satisfying all of the optical requirements of the Pockel cell when used with the lidar receiving system. Preliminary designs coupled with some detailed discussions with manufacturers of Pockel cells have indicated a feasible Pockel cell configuration which should allow attenuation of the plume return signal by a factor of at least 100. Such an attenuation should reduce afterpulsing to the point of its error contribution being negligible. This technique can then be considered as a back-up to the previous technique of employing a gridded photomultiplier tube.

Following the completion of either or both of the above modifications it would be desirable to evaluate the effect of these changes using the synthetic targets at approximately 200 to 300 meters range. This would not be difficult since the targets exist and have been calibrated, and if the r^2 compensation has been installed data reduction will be much less time consuming. Of course, a limited number of shots would probably be made using the existing lidar configuration for side by side comparison and these would be time consuming to process.

Finally, it is recommended that the problem of thermal lensing of smoke plumes be investigated both analytically and experimentally. A first order analysis should

be made for the case of laminar plumes to indicate the effective focal length of such lenses and the variation of this focal length across the plume allowing for temperature gradients. This would then be inserted into a simple optical model of the lidar transmitted pulse and receiver field of view allowing first order numerical evaluation of the lensing effect. Experimental confirmation of these results could then be gotten by systematically observing highly transmitting, hot, laminar plumes and comparing the far side signal return both through and immediately adjacent to the plume. As has been mentioned earlier it does not look reasonable to analyze turbulent plumes but systematic lidar observations could be made, perhaps with varying receiver fields of view, both through and adjacent to the plume yielding a better measure of the frequency of and factors contributing to lack of far side $1/r^2$ performance.

7. ACKNOWLEDGEMENTS

The authors are grateful for the cooperation of the Philadelphia Electric Company and the Allegheny Power and Light Company for making their power station facilities available for the field testing done during the evaluation of the mobile lidar system.

8. REFERENCES

1. Conner, W. D. and Hodkinson, J. R., "Optical Properties and Visual Effects of Smoke Stack Plumes", Public Health Service Publication No. 999-AP-30, Cincinnati, Ohio, 1967.

2. Evans, W. E., "Development of Lidar Stack Effluent Opacity Measuring System", Final Report of Stanford Research Institute Project No. 6529, Menlo Park, California, July 1967.

3. Bethke, G. W., Cook, C. S., and Mezger, F. W., "Laser Air Pollution Probe", Final Report, ARC Contract No. 68-19, January 1970.

APPENDIX A

THE LIDAR RANGE EQUATION

It is assumed that the laser light source is pulsed, with light pulses which are short in length compared to the measurement ranges of interest. It is also assumed that the laser beam is collimated to a divergence which is smaller than the lidar receiving system angle of acceptance (field of view). It is further assumed that the transmitted laser beam is coaxial or nearly coaxial with the receiving system, such that the propagating laser beam is located entirely within the receiving system field of view during the period (ranges) of interest. Because the laser beam is located entirely within the receiver field of view, only the total power (P_L) and energy (E) of the laser beam need be considered, and not the beam intensity.

The total power of incident light (P_i) scattered in direction θ by illuminated scattering length (ℓ) of gas is

$$P_s(\theta) = P_i \ell \cdot k_s(\theta) \qquad (1)$$

where $k_s(\theta)$ is the directional scattering coefficient.

Now referring to Figure A-1, we see that a pulse of light which starts from the laser at time t_o and continues to be emitted until time t_L, has a length L, where

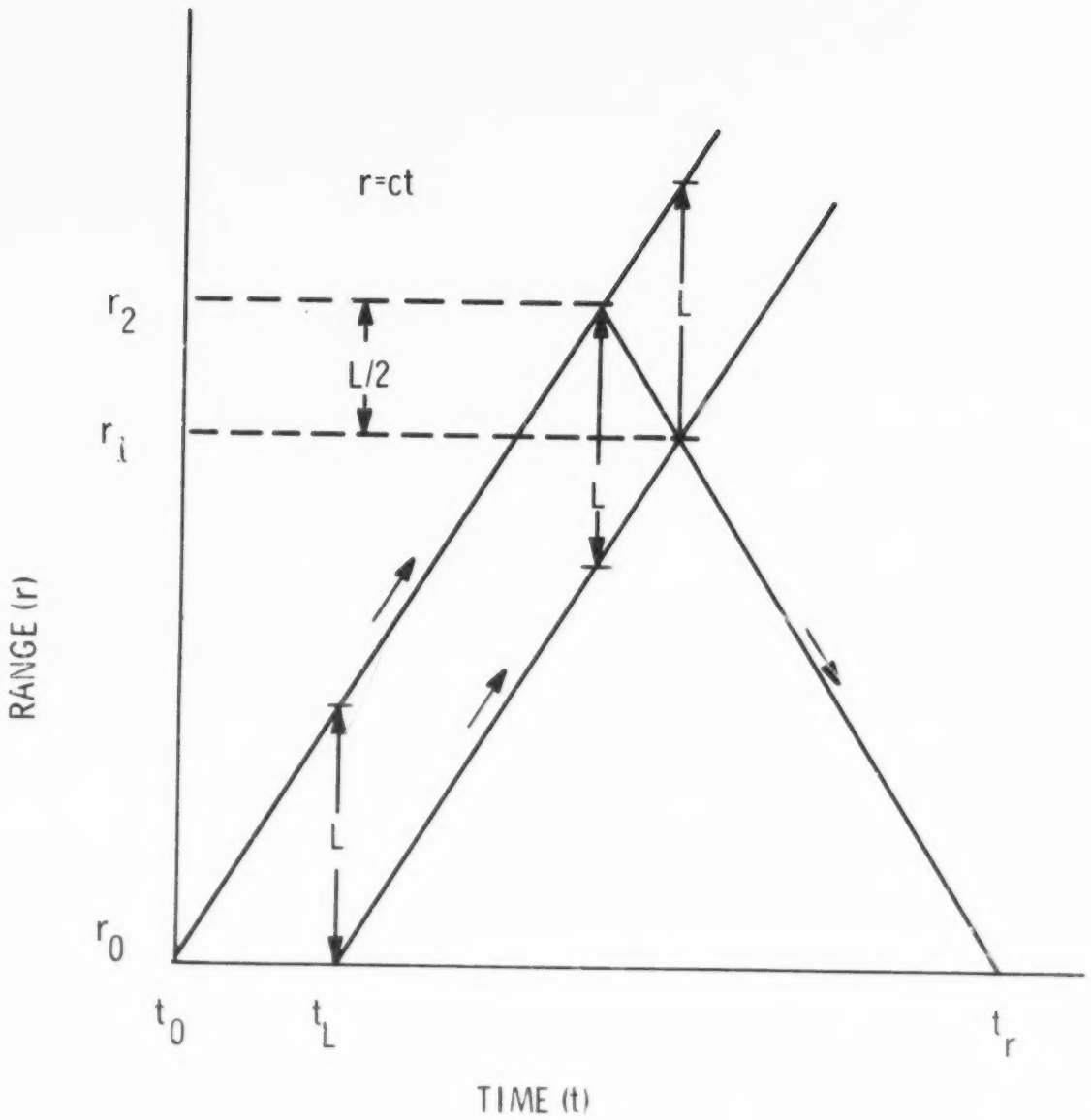

Figure A-1. Laser pulse range vs. time diagram. This diagram illustrates the length (L/2) of the lidar system laser pulse scattering volume which is observed at time t_r, for a laser pulse of length L.

$$L = c\,(t_L - t_o) = c\,t_L \qquad (2)$$

As this short light beam of length L propagates away, light is continuously scattered back to the lidar system. However, Figure A-1 illustrates that the scattered light observed by the lidar system at any one instant in time, t_r, is scattered only from incident light located between ranges r_1 and r_2 which have a distance difference of L/2. Thus the illuminated length of gas that scatters light back towards the lidar system at any one time, t_r, is

$$\ell = r_2 - r_1 = L/2. \qquad (3)$$

The light which left the lidar laser with power P_L arrives at the range of interest (r) with reduced incident power P_i due to atmospheric extinction. Thus

$$P_i = P_L \exp(-r k_e) \qquad (4)$$

where k_e is the total extinction coefficient of air from all sources assuming extinction to be constant with range. Finally,

$$P_L = \dot{E} = E/t_L \qquad (5)$$

where E is the total laser energy per pulse. Now combining equations 1 through 5, we have

$$P_s(\theta) = (c E \cdot k_s(\theta)/2) \exp(-r k_e). \qquad (6)$$

The power of back-scattered light collected (P_c) by the lidar receiving objective is

$$P_c = P_s(180^\circ) \cdot \Gamma \exp(-r k_e) \qquad (7)$$

where Γ is the solid angle subtended by the lidar receiving objective from the scattering range r. But

$$\Gamma = 2\pi(1 - \cos\gamma) \approx \pi\gamma^2 \approx A/r^2 \tag{8}$$

where γ is the angle subtended by the radius of the lidar receiving objective from scattering distance r, and A is the area of the receiving objective. Since it has been assumed that the light pulse is short in length compared to the measurement ranges of interest, we can assume with negligible error that Γ is the same at any one instant (t_r) from all portions of the illuminated scattering volume. Finally, the power of scattered light which reaches the detector (P_d) is

$$P_d = E_o P_c \tag{9}$$

where E_o is the total efficiency of all optics in both the transmitting and receiving sections of the lidar system. Thus combining equations 6 through 9 we have

$$P_d = \frac{c}{2} \frac{A}{r^2} E_o E \cdot k_s (180^\circ) \cdot \exp(-2r k_e) . \tag{10}$$

If P_d is in watts and the detector has a sensitivity S in amps/watt, then the voltage drop, V, produced by detector output current I across detector load resistor R is

$$V = IR = P_d S R \tag{11}$$

The directional scattering coefficient consists of both molecular (Rayleigh) scattering, and particulate or aerosol (Mie) scattering.

$$k_s(\theta) = n(r) \cdot \sigma_R(\theta) + m(r) \cdot \sigma_M(\theta) \tag{12}$$

Here, n is the molecular concentration (density) in air, $\sigma_R(\theta)$ is the directional Rayleigh cross section, m is the particulate concentration in air, and $\sigma_M(\theta)$ is the suitably size-integrated directional Mie theory-calculated cross section for particulates in the air.

Similarly, the total extinction coefficient is defined as molecular (Rayleigh) and particulate or aerosol (Mie) total scattering plus any molecular absorption at the specific wavelength of interest.

$$k_e = n(r) \cdot \sigma_R + m(r) \cdot \sigma_M + k_a \qquad (13)$$

Here σ_R is the total Rayleigh cross section, k_a is the absorption coefficient of air at the laser wavelength and σ_M is the total particulate (Mie) cross section. As is clear from equation 13, k_e is not constant with range. Consequently, we must replace the expression $(r k_e)$ in equations 4, 6, 7, and 10 with

$$r k_e \rightarrow \sigma_R \int_o^r n(r) dr + \sigma_M \int_o^r m(r) dr + r k_a . \qquad (14)$$

Finally, combining equations 10, 11, 12, and 14, one obtains the range equation

$$V = cR\, SE_o \frac{EA}{2r^2} \left[n(r) \cdot \sigma_R(180^\circ) + m(r) \cdot \sigma_M(180^\circ) \right] \cdot \exp -2 \left[\sigma_R \int_o^r n(r) dr + \sigma_M \int_o^r m(r) dr \right] . \qquad (15)$$

Here we have dropped the absorption coefficient of equation 14 because

we assume that the laser wavelength does not coincide with a significant atmospheric line or continuum.

atmospheric density, n can be expressed analytically if one curv[illegible]s to a suitable standard atmosphere. For lidar system elevations that do not cover a range of more than a few thousand feet above sea level, the following expression is useful to about 50,000 feet scattering altitude:

$$n = n_o \frac{T_o p}{T_{po}} \cdot \left[\exp\left(-2.3026 \frac{r}{Z'} \sin\varphi\right) - Z'' r^2 \sin^2\varphi\right] \qquad (16)$$

Here, n_o is the value of n at temperature T_o and pressure p_o, while T is air temperature and p is air pressure near the lidar system, φ is the lidar system angle of elevation above horizontal, and Z' and Z'' are suitable constants. If the lidar system is at sea level and r is in cm, then setting $Z' = 2.31 \times 10^6$ cm and $Z'' = 3.0 \times 10^{-14}$ cm^{-2} gives n values which agree with the AFCRL 1959 standard atmosphere to within $\leq 0.6\%$ and $< 3\%$ at $\leq 30,000$ feet and $< 50,000$ feet altitudes above the lidar, respectively. If the lidar system is at 2000 feet altitude, then the same assumptions give agreement to within $\leq 1\%$ and $< 6\%$ at $\leq 20,000$ feet and $\leq 50,000$ feet altitudes above the lidar, respectively. Of course for $\varphi << 90^o$, one is not concerned with such high altitudes even when r is large.

APPENDIX B - PHOTOMULTIPLIER TUBE GATING INVESTIGATIONS

In order to make lidar-determined smoke plume transmittance measurements, it is necessary to faithfully record the atmospheric backscattering both just in front of and just behind the plume. There is, of course, no trouble in obtaining the near side signal right up to the point in time where the laser pulse intersects the plume. However, the intense light scattering from the plume itself (during the time that the laser pulse is in the plume) complicates the problem of faithfully recording the clear air light scattering immediately on the far side of the plume. This backscattering from the plume can be as high as 40 db above the ambient clear air scattering for the case of a dense white plume (or for test purposes, a white wall).

Two separate after effects from this intense plume signal can occur during the time period just following the emergence of the laser pulse from the plume. Both of these effects tend to increase the apparent amplitude of the far side clear air return, yielding transmittance values for the plume that are too high.

The first effect is simply caused by the frequency response of the detector and amplifying electronics in going from the high level plume signal to the low level far side clear air signal. Since the slowest frequency response occurs in the amplifying electronics, turning off the detector during the intense plume return will avoid overdriving the electronics and will allow a proper far side measurement.

The second effect is called after-pulsing and is less certain in origin although its effects are obvious. Each strong discrete light pulse (plume signal) produces

not only a corresponding discrete output from the photomultiplier tube (PMT) anode, but also one or more secondary output pulses which usually occur 0.2 to 1 microsecond after the primary pulse. These secondary pulses are somewhat broader and decay much more slowly than the main pulse. The explanation for this effect is as follows: The PMT cathode photoelectrons (created by backscattered light from the intense plume return) leave the cathode and are accelerated towards the first dynode. At some point along their path these electrons acquire sufficient energy to ionize the residual gas in the tube or to eject ions from the tube structure upon impact. These relatively slow ions then are accelerated back to the photo-cathode where they cause secondary electron emission. The secondary electrons then are amplified down the dynode chain and wind-up as an after-pulse signal at the anode. Those electrons resulting from light ion impact at the photocathode cause the earliest after-pulsing while heavier and slower ions cause the later after-pulsing. The amount of after-pulsing then depends on the intensity of the reflected signal from the plume or target.

To eliminate at least the first (slow electronics recovery) effect and if possible also the afterpulsing effect, investigations were made to determine the best method for gating off the PMT during receipt of the strong smoke plume return. The various requirements imposed on the off-gate method to be used included the need for a large on/off ratio (preferably > 30 db), a rapid off-gate response and rapid on-recovery response (< 100 nanoseconds), and the ability to off-gate for at least 200 nanoseconds. The real thickness of smoke plumes combined with the total time of the complete laser pulse, all under field operating conditions, imposes the last requirement.

EXPERIMENTAL TEST METHODS

Several experimental methods were used to measure the above-mentioned gating characteristics as a function of the gating method being tried. In all cases, the PMT operating voltage was set to the value anticipated for lidar operation. Also, a Tektronix #551 oscilloscope with H preamplifer was used for all the response time measurements, this combination having a manufacturer - stated risetime of 25 nanoseconds. The pulse generator provided pulses of $< \pm 100$ volts, with 15 nanosecond rise and fall times.

PMT gating response time and the smaller on/off ratios (< 25 db) were measured by off-gating the PMT while it was exposed to a cw light source. In these cases, a Corning #2412 red filter was used and the light level was adjusted to yield PMT anode outputs less than 0.1 of the divider chain current. The latter precaution insured linear PMT response under cw operating conditions.

The larger on/off ratios (> 25 db) which resulted from off-gating the PMT were measured with a pulsed red light source as follows: A He - Ne laser (6328 A) was beamed at a rotating prism (500 rps) which swept the reflected laser beam across an 18 foot distant aperture placed in front of the PMT. An opal glass diffuser between the aperture and the PMT produced nearly uniform illumination of the PMT photocathode as the laser beam moved across the aperture, thus minimizing the effect of any spatial nonuniformities in the photocathode sensitivity. Whenever it was necessary to reduce the light intensity on the PMT by a known amount, calibrated neutral density filters were placed in front of the aperture. For most of these measurements, the aperture was set so the light pulses were about 0.3 to 0.4 microseconds long (FWHH). For these measurements, the PMT

anode maximum current, maximum current times pulse width (charge/pulse), and average current were all kept within linear response ranges for the PMT. The linearity between PMT anode pulse amplitude and input light pulse intensity was determined using this same experimental set-up at (a) constant light level while varying PMT voltage and (b) constant PMT voltage while varying light level via calibrated neutral density filters.

Finally, afterpulsing plus any electronics effects were measured with the PMT in the lidar system. The lidar return from a white wall plus the laser output energy monitor signal were displayed on the lidar oscilloscope, both with and without off-gating the PMT during the white wall return. This very strong and brief light return approximated that which would be returned from a dense white (high reflectance) smoke plume, a very severe test. Since the wall was opaque, the signal level ideally should have gone to zero immediately after the wall return signal. Any remaining non-cw PMT signal was then due to a combination of PMT afterpulsing plus any effects originating in the receiver electronics.

OFF-GATING METHODS AND RESULTS

Our investigations have included off-gating the Amperex 56 TVP PMT via (a) the focus electrode, (b) the photocathode (by pulsing an external wire mesh), (c) dynode 2, (d) dynode 6, and (e) dynodes 2 and 6 simultaneously. The RCA 7265 PMT fits the same socket as the Amperex tube, with most of the pin connections being the same as well as having a very similar voltage distribution requirement. Thus the divider circuit was only slightly modified for the RCA 7265 PMT which was also investigated while off-gating via (a) the focus electrode, (b) the photo-

cathode (using an external mesh), and (c) dynodes 2 and 6 simultaneously.

The principal results of all these investigations are summarized in Table B-I which lists the PMT used, the pulsed element, the pulse voltages for best gating characteristics (within + 100 V to - 100 V limits), the 0% to 90% turn-on response time at the end of a 200 nanosecond(off-gating) pulse period, and the on/off gating ratio for both the primary (plume) signal and for the resulting afterpulse signal. Since the on-response time increases with pulse width for some of the gating methods, a 200 nanosecond pulse period is used for comparison in Table B-I, that being the shortest off-gating period that is usually practical under field conditions while looking at real smoke plumes.

During these investigations, for each PMT driving voltages were used which yielded PMT gains approximately those which were later found to be needed for lidar use. (Lidar use required 1500 V for the Amperex 56 TVP tube and 1900 - 2000 V for the RCA 7265 tube). The PMT voltage divider used for all these investigations had resistor (R) ratios as follows: focus electrode adjustable, cathode -D1 = 3R, D1 - D2 through D10 - D11 = R, D11 - D12 = 1.36R, D12-D13 = 2R, D-13 - D14 = 3R, and D14 - ground = 4R.

Based on the afterpulse mechanism suggested earlier, it would appear that off-gating a PMT by reversing the electric field at or near the photocathode surface would eliminate any afterpulsing (to the extent of the on/off ratio) since ionization then could never occur in the region beyond the photocathode. For this reason and also because of earlier work and suggestions by Evans[1], the initial attempts were to off-gate the Amperex 56 TVP PMT first via the focus electrode

and then via an external metal mesh over the photocathode. The results of these plus subsequent investigations are described in the following subsections.

Afterpulsing and Focus Electrode Gating of the Amperex 56 TVP

As shown in Table B-I, when off-gating was accomplished using the focus electrode of the Amperex 56 TVP PMT, the best results were obtained by employing a -100 V pulse. Under these conditions, the afterpulsing was reduced by about 8 db. However, the PMT recovery time at the end of the off-gated period was too slow to be useful for the plume opacity measurement application.

Figure B1a shows the non-gated Amperex 56 TVP afterpulsing resulting from the lidar being shot at a white wall, while Figures B1b and B1d show the reduced afterpulsing obtained when the source (wall backscatter) signal was gated off with a -100 V pulse to the PMT focus electrode. As seen from Figure B1a, the principal afterpulse maximum (A) is 0.67 μ sec after the source pulse (W), while a secondary afterpulse (A′) is 1.3 μ sec after W. The principal afterpulse is about 40 db less than the source pulse would be if the PMT did not saturate. Between A and W (Figure B1) there is a reduced level of signal which is still non-zero. Since an opaque wall permits no lidar return from greater ranges, a perfect detector would show zero return after W.

Table B-I also shows the on-response time to be an undesirably slow 630 n sec when a -100 V 200 nsec wide gating pulse was applied to the PMT focus electrode. This is the narrowest gate width practical for field use on real plumes. These on-response times were found to increase considerably with increasing pulse width and with increasing absolute value of pulse voltage on the focus electrode,

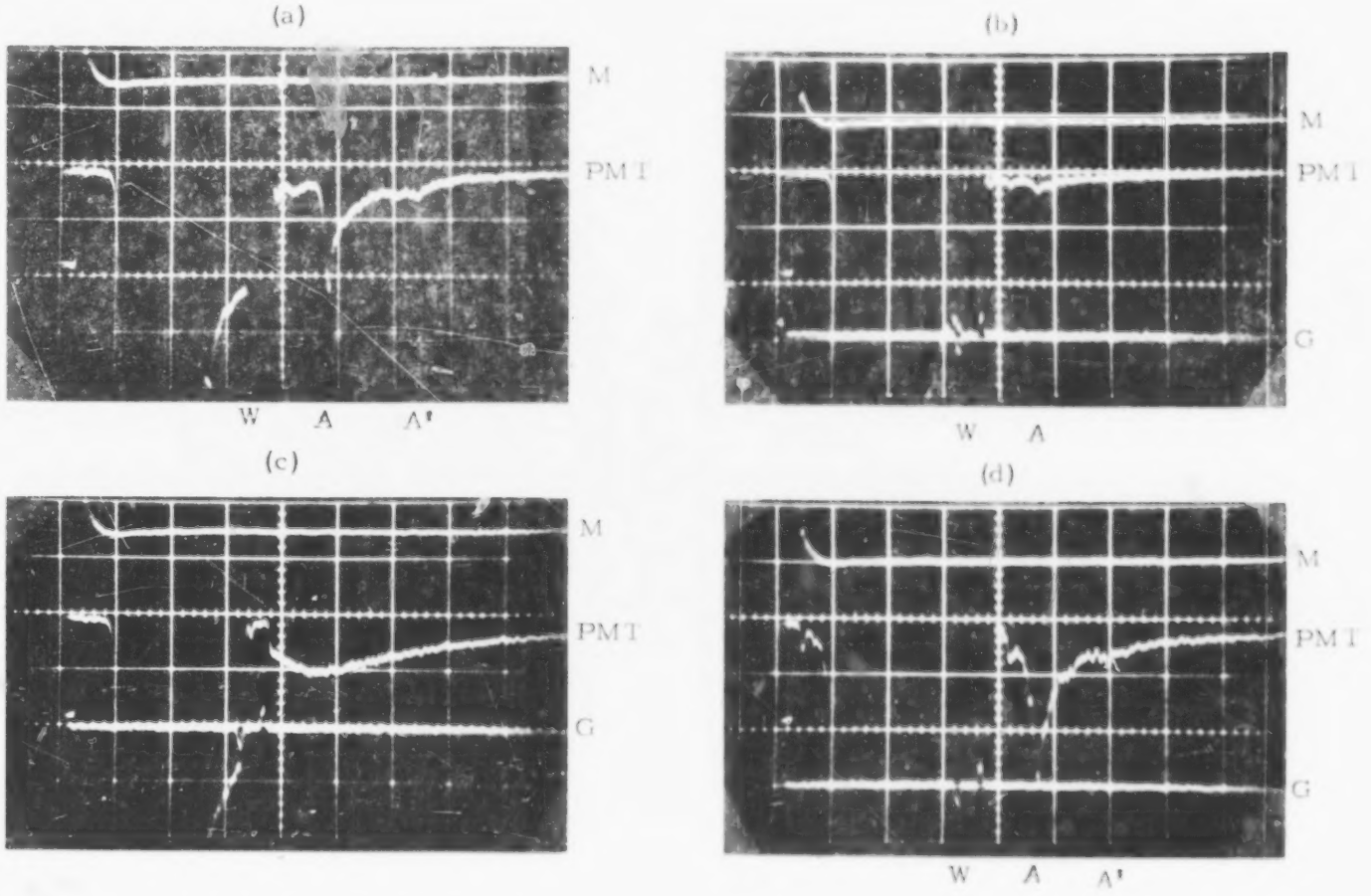

Figure B1. Lidar oscillograms showing the results when the PMT detector is an Amperex 56 TVP with focus electrode gating and with the following conditions: B1a is white wall target and no gate, B1b and B1d are white wall target with gate, and B1c is no target but with gate. In each oscillogram, W is position of wall return, A and A′ are afterpulse peaks, M is the laser energy monitor trace, PMT is the PMT lidar return (negative going signal), and G is the differentiated off-gating pulse showing gate position. In all cases, the gate pulses are -100 V amplitude and 200 nsec wide, oscilloscope sweep speeds are 0.5 μsec/cm, and the PMT traces are 0.5 V/cm except for 0.05 V/cm for PMT of Figure B1d.

Table B-I. Photomultiplier Tube Off-Gating Characteristics

Tube Used	Element Pulsed	Pulse voltage	On-response time (n sec.) (a)	On/off ratio (db) Source signal	On/off ratio (db) Afterpulse maximum
Amperex 56 TVP (c)	Focus electrode	+ 100 V	610 n s	11db	0 db
	Focus electrode	- 100	630	~23	~8
	Photocathode[b]	+ 60	930	18	---
	Photocathode	- 40	2000	8.2	---
	Dynode 2	+ 100	~ 40	20	---
	Dynode 2	- 100	---	15	---
	Dynode 6	+ 100	~ 30	23	---
	Dynode 6	- 100	~ 30	25	---
	Dynodes 2 & 6	+ 100	~ 35	45	0
	Dynodes 2 & 6	- 100	~ 40	41	~0
RCA 7265 (d)	Focus electrode	+ 100	~ 130	14	0
	Focus electrode	- 100	~ 130	11	0
	Photocathode[b]	+ 100	1800	>13	---
	Photocathode	- 70	1000	7.0	---
	Dynodes 2 & 6	+ 100	~ 50	45	0
	Dynodes 2 & 6	- 100	~ 50	36	---

(a) Gating pulses were 200 nanoseconds wide.

(b) The photocathode was pulsed capacitively by pulsing an external wire mesh which was held flat against the face of the tube.

(c) Amperex tube was operated at 1300 and 1500 volts.

(d) RCA tube was mostly operated at 1900 and 2000 volts.

and to decrease somewhat with increasing total operating voltage on the PMT. For example, for 1500 V on the PMT and -100 V pulses, the PMT on-response time at the end of the off-gate period increased from 350 nsec for 100 nsec pulse widths, to 630 nsec for 200 nsec pulse widths, and to 1100 nsec for 500 n sec pulse widths. Figure B1c illustrates the effect of the slow on-response recovery of the Amperex PMT when focus electrode gating was employed. Since here the lidar shot was into clear air, the PMT output should have resumed its $1/r^2$ fall-off immediately at the end of the 200 nsec gate.

Afterpulsing and Focus Electrode Gating of the RCA 7265

When off-gating at the focus electrode of the RCA 7265 PMT, the best results were obtained with + 100 volt pulses. Unlike the Amperex tube, this RCA PMT showed a usefully rapid 0% - 90% on-response (recovery) time of ~ 130 nsec after any gating pulse < 1000 nanoseconds wide. Unfortunately, gating at the RCA PMT focus electrode had no attenuating effect on its afterpulsing. These results are summarized in Table B-I.

Figure B2 is a lidar oscillogram showing afterpulsing by an ungated RCA 7265 PMT. This oscillogram resulted from a lidar shot at a white wall, with the wall return being located at W on the oscillogram. The principal afterpulse maximum (A) is about 0.3 μ sec after W, followed by a strong secondary afterpulse (A ′) about 1 μ sec after W. Here too, the strongest afterpulse maximum was about 40 db less than the source pulse would have been if the PMT did not saturate. Between W and A, and betwen A and A′ there are reduced signal levels which are still non-zero. Although the timing and detailed shape of afterpulsing from

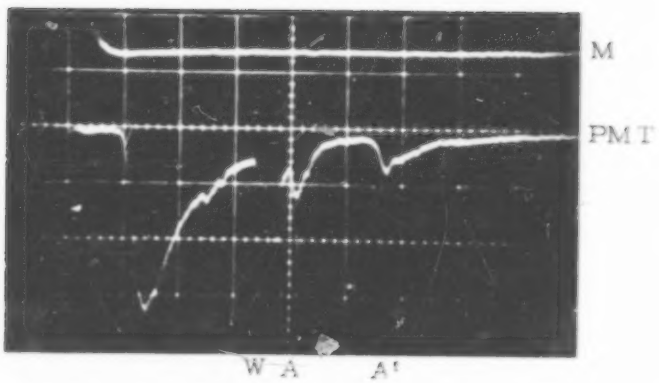

Figure B2. Lidar oscillogram showing RCA 7265 photomultiplier tube (PMT) afterpulsing. Trace M is the positive-going laser energy monitor output and trace PMT is the negative-going PMT output. The lidar shot is at a white wall target with its off-scale return at W, and the resulting afterpulse peaks at A and A′. Oscilloscope sweep speed is 0.5 μ sec/cm.

the RCA PMT are different than that from the Amperex PMT, the magnitude of afterpulsing from both PMT's is comparable.

External Grid Gating of the Amperex 56 TVP

When pulsing the Amperex PMT photocathode by means of an external mesh grid held flat against the face of the tube, as shown in Table B-I the best off-gating was obtained with a + 60 volt pulse. However, the PMT recovery time at the end of the off-gated period was far too slow to be useful. Consequently, the afterpulse on/off ratio was not measured.

As with the Amperex tube focus electrode gating already discussed, when the Amperex PMT was capacitively gated at its photocathode via an external mesh the on-response (recovery) times were found to increase considerably with increasing pulse width and with increasing absolute values of pulse voltage. The effect of pulse width on PMT recovery time is shown in Figure B3 which shows PMT output while exposed to cw light and being gated off with +60 volt pulses applied to the external mesh. For this type of oscillogram, the PMT output (upper trace) is a negative-going signal which shows some ringing as each pulse (lower trace) starts and ends. The effects of three pulse widths (200, 500, and 1000 nsec are superposed, with the slow on-recovery of PMT sensitivity being apparent at the end of each pulse. In this way, 0% - 90% recovery times from + 60 V pulses were found to be ~ 0.23, 0.9, 2.5, and > 3.5 μ sec for 0.1, 0.2, 0.5, and 1.0 μ sec wide pulses, respectively.

External Grid Gating of the RCA 7265

As listed in Table B-I, the results of off-gating at the photocathode of the RCA

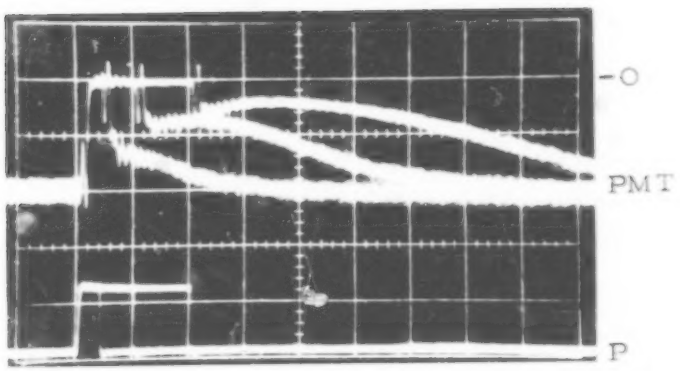

Figure B3. Oscillogram showing Amperex 56 TVP photomultiplier tube (PMT) output while exposed to cw light and being gated off with pulses capacitively applied to its photocathode via an external mesh grid. The three overlapping lower traces (P) show the +60 V gating pulses of 200, 500, and 1000 nsec width which are applied to the PMT. The three partly overlapping upper traces (PMT) show the PMT output and its recovery to full sensitivity after the off-gating pulses end. The PMT traces are negative-going, with their zero at 0. Sweep speed is 0.5 μ sec/cm, and vertical sensitivities are 5 mV/cm for PMT and 50 V/cm for P.

7265 PMT by pulsing an external mesh grid held flat against the face of the tube, show the PMT recovery at the end of the off-gated period to be too slow to be useful. Thus, the afterpulse on/off ratio was not measured.

In this case as with the Amperex tube, the recovery times were found to increase considerably with increasing pulse width and with increasing absolute values of pulse voltage. Even for -70 V gating pulses (PMT at 2000 V), the 0% - 90% recovery times were found be ~ 0.53, 1.0, 1.4, and 1.6 μ sec for 0.1, 0.2, 0.5, and 1.0 μ sec wide pulses, respectively.

Dynode Gating of the Amperex 56 TVP

Primarily because of the excessively slow recovery of PMT sensitivity after off-gating via both focus electrode and external mesh over the photocathode, other means were sought for gating the PMT. Consequently, off-gating pulses were applied to dynodes 2, 6, and 2 + 6 with the results summarized in Table B-I and detailed below.

When dynodes 2 and 6 were separately pulsed with ± 100 volts, the Amperex tube was found to be gated off with on/off ratios of 15 - 25 db (see Table B-I). In all of these cases, the on- (and off-) response times were measured as < 40 nanoseconds for off-gate periods of 200 nanoseconds.

Subsequently, ± 100 volt off-gate pulses were simultaneously applied to both dynodes 2 and 6 of the Amperex 56 TVP tube, resulting in the following on/off ratios for various operating conditions:

PMT volts	Pulse volts	On/off ratio
1300	+ 100 V	46.2 db
1300	- 100	39.1 db
1500	+ 100	45.4 db
1500	- 100	40.7 db
1900	+ 100	43.5 db
1900	- 100	40.7 db

The PMT on- (and off-) response times were found to be < 40 nsec for off-gate periods < 500 nsec. This response can be seen in Figure B4 which shows the response by the PMT to off-gating in the presence of the cw light source. At the high oscilloscope sensitivity needed to show PMT cw output with fast response (93 ohm cable and load), PMT anode stray pickup from the gating pulse produced 10 mV spikes in the PMT anode signal corresponding to the beginning and end of each gate pulse. These pickup spikes do not interfere with lidar useage of the detector due to their very transient nature and due to the fact that lidar shots use oscilloscope sensitivities 10 to 200 times lower than used in Figure B4. Figure B5 also shows the fast response obtained by off-gating the Amperex 56 TVP via dynodes 2 plus 6, this figure being an oscillogram of a no target lidar shot taken through the clear aperture of the synthetic target holders (see Section 3).

As indicated in Table B-I, the PMT afterpulse maxima were not influenced by gating off the source signal via dynodes 2 plus 6. However, lidar system evaluation tests using known synthetic targets (see Section 3 of the report) show that target transmittance measurements made during the afterpulse minimum between the source (target) signal and the first afterpulse maximum (W and A of Figure B1a), are much more accurate with dynode 2 plus 6 off-gating than without such off-gating. As discussed in the report, this difference may be due to the ungated intense target return overdriving the detection system electronics.

Finally, the question arose as to whether the afterpulsing was superlinear, such that its amplitude would fall off faster than that of the source intensity if the source intensity were reduced. To check this possibility, additional lidar measurements were made of afterpulsing while varying the source (wall return)

The PMT on- (and off-) response times were found to be $\leq$ 40 nsec for off-gate periods $\leq$ 500 nsec. This response can be seen in Figure B4 which shows the response by the PMT to off-gating in the presence of the cw light source. At the high oscilloscope sensitivity needed to show PMT cw output with fast response (93 ohm cable and load), PMT anode stray pickup from the gating pulse produced 10 mV spikes in the PMT anode signal corresponding to the beginning and end of each gate pulse. These pickup spikes do not interfere with lidar useage of the detector due to their very transient nature and due to the fact that lidar shots use oscilloscope sensitivities 10 to 200 times lower than used in Figure B4. Figure B5 also shows the fast response obtained by off-gating the Amperex 56 TVP via dynodes 2 plus 6, this figure being an oscillogram of a no target lidar shot taken through the clear aperture of the synthetic target holders (see Section 3).

As indicated in Table B-I, the PMT afterpulse maxima were not influenced by gating off the source signal via dynodes 2 plus 6. However, lidar system evaluation tests using known synthetic targets (see Section 3 of the report) show that target transmittance measurements made during the afterpulse minimum between the source (target) signal and the first afterpulse maximum (W and A of Figure Bla), are much more accurate with dynode 2 plus 6 off-gating than without such off-gating. As discussed in the report, this difference may be due to the ungated intense target return overdriving the detection system electronics.

Finally, the question arose as to whether the afterpulsing was superlinear, such that its amplitude would fall off faster than that of the source intensity if the source intensity were reduced. To check this possibility, additional lidar measurements were made of afterpulsing while varying the source (wall return)

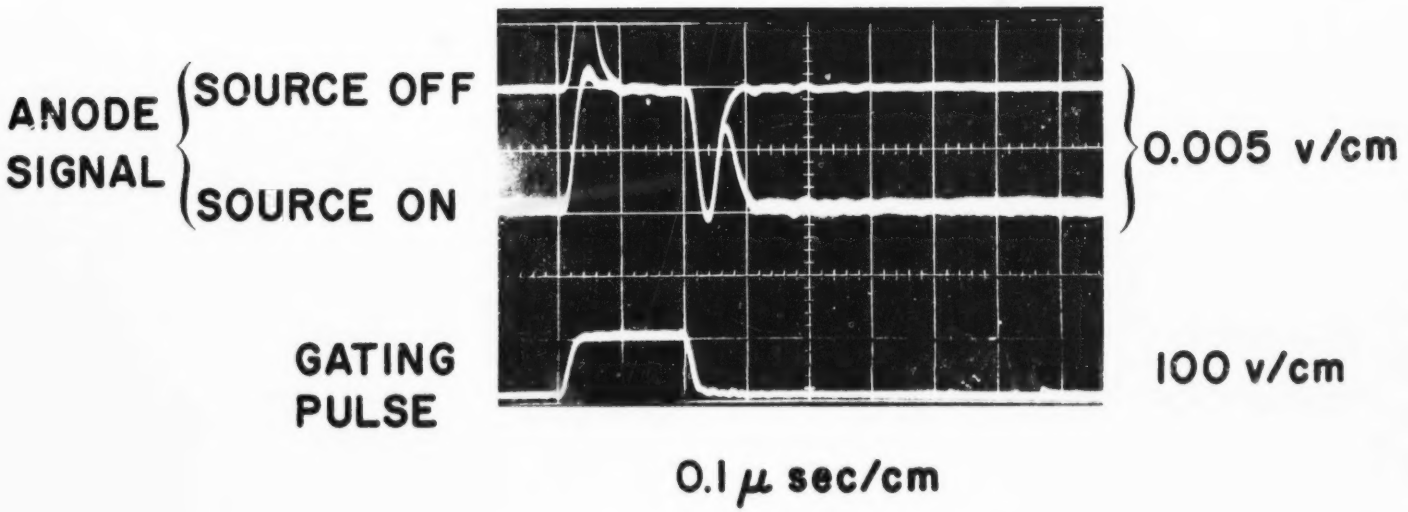

Figure B4. Oscillogram showing response by the Amperex 56 TVP photomultiplier tube to simultaneous off-gating at dynodes 2 and 6 in the presence of a cw light source. The anode trace has an oscilloscope risetime of 25 nsec, while the gating pulse trace has an oscilloscope risetime of 13 nsec.

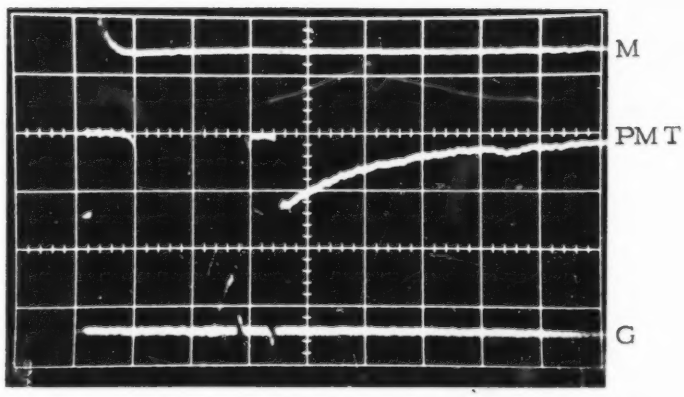

Figure B5. Lidar oscillogram showing response by the Amperex 56 TVP photomultiplier tube (PMT) to simultaneous off-gating at dynodes 2 and 6. This lidar shot was made through the clear aperture of the synthetic target holders into clear air while being gated off with a 300 nsec wide + 100 V pulse. Here, M is the positive-going laser energy monitor trace, PMT is the negative-going PMT lidar return, and G is the differential off-gating pulse showing gate position. Oscilloscope sweep speed is 0.5 μsec/cm.

intensity and off-gating the Amperex tube at dynodes 2 plus 6. While operating the lidar laser at a constant output, the afterpulsing resulting from the off-gated white wall return was investigated employing various masks (1.0, 0.1 and 0.01 area) over the lidar receiving system objective. Varying the receiving aperture area over a factor of 100 resulted in no significant change in the ratio of source intensity (on PMT) to afterpulse peak signal or the ratio of source intensity (on PMT) to afterpulse minimum located before the afterpulse peak (see Fig. B1a). Thus, afterpulsing appears to be a linear function of the source pulse, as the proposed afterpulse mechanism would suggest.

Dynode Gating of the RCA 7265

As shown in Table B-I, when off-gating the RCA 7265 PMT by simultaneously pulsing both dynodes 2 and 6, the PMT on/off ratio was large enough (45 db at 1900 V and + 100 V pulses) and the PMT speed of recovery from the off-gate condition was fast enough (about 50 nsec) to be useful. As with similar gating of the Amperex tube, the afterpulse maximum was not reduced by dynode gating.

DISCUSSION AND CONCLUSIONS

It has been determined that off-gating the Amperex 56 TVP PMT at either the focus electrode or at the photocathode (via an external mesh grid), and also the RCA 7265 PMT at the photocathode (via an external mesh) all result in a fast off-gate response, but much too slow a subsequent on-recovery to be useful for lidar transmittance measurements of real plumes under field conditions. This slow on-recovery of the PMT's after off-gating at or near the photocathode is probably due to the slow redistribution of charge on the semiconducting trialkali photocathode after the off-gate ends. The longer the off-gate pulse lasts, the longer

the photocathode is exposed to altered electric fields, resulting in the accumulation of greater deviations from the normal charge distribution. The difference in this recovery time characteristic between the Amperex and the RCA tubes when using focus electrode gating, is probably due to their differences in focus electrode design and its closeness to the photocathode.

Although the RCA 7265 tube showed fairly fast off- and on- response when off-gating at the focus electrode, its on/off ratio was not very good and the off-gate did not reduce the afterpulsing.

The dynode methods of off-gating both the Amperex and RCA tubes all show both fast off-gate response and subsequent fast on-recovery because the dynodes have highly conducting metal substrates and are well removed from influencing the electric field around the semiconducting photocathode.

It was decided to use simultaneous + 100 volt pulsing of both dynodes 2 and 6 to off-gate the PMT because this method produced the fastest off- and on-response and the largest on/off ratio when off-gating. Given this dynode 2 plus 6 method of off-gating, the Amperex 56 TVP tube was selected because its afterpulsing became increasingly strong only at >550 nsec after the target (plume) return, while the RCA 7265 tube showed strong afterpulsing starting much closer (about 200 nsec) to the target return signal. Thus, the Amperex PMT permits the far-side-of-plume measurement to be made immediately (<550 nsec) after the plume signal where afterpulsing effects are relatively weak.

REFERENCES

1. W. E. Evans, "Development of Lidar Stack Effluent Opacity Measuring System", Stanford Research Institute report, SRI Project 6529, July 1967.